

A vertebra of a small species of Pachycetus from the North Sea and its inner structure compared with other basilosaurid vertebrae from the same site. (#86691)

1

First submission

Guidance from your Editor

Please submit by **7 Aug 2023** for the benefit of the authors (and your token reward) .



Structure and Criteria

Please read the 'Structure and Criteria' page for general guidance.



Author notes

Have you read the author notes on the [guidance page](#)?



Raw data check

Review the raw data.



Image check

Check that figures and images have not been inappropriately manipulated.

If this article is published your review will be made public. You can choose whether to sign your review. If uploading a PDF please remove any identifiable information (if you want to remain anonymous).

Files

Download and review all files from the [materials page](#).

23 Figure file(s)

5 Table file(s)




Structure and Criteria

Structure your review

The review form is divided into 5 sections. Please consider these when composing your review:

1. BASIC REPORTING
2. EXPERIMENTAL DESIGN
3. VALIDITY OF THE FINDINGS
4. General comments
5. Confidential notes to the editor






 You can also annotate this PDF and upload it as part of your review

When ready [submit online](#).





Editorial Criteria

Use these criteria points to structure your review. The full detailed editorial criteria is on your [guidance page](#).




BASIC REPORTING

-  Clear, unambiguous, professional English language used throughout.
-  Intro & background to show context. Literature well referenced & relevant.
-  Structure conforms to [PeerJ standards](#), discipline norm, or improved for clarity.
-  Figures are relevant, high quality, well labelled & described.
-  Raw data supplied (see [PeerJ policy](#)).

EXPERIMENTAL DESIGN

-  Original primary research within [Scope of the journal](#).
-  Research question well defined, relevant & meaningful. It is stated how the research fills an identified knowledge gap.
-  Rigorous investigation performed to a high technical & ethical standard.
-  Methods described with sufficient detail & information to replicate.

VALIDITY OF THE FINDINGS

-  Impact and novelty not assessed. *Meaningful* replication encouraged where rationale & benefit to literature is clearly stated.
-  All underlying data have been provided; they are robust, statistically sound, & controlled.
-  Conclusions are well stated, linked to original research question & limited to supporting results.



The best reviewers use these techniques

Tip

Example

Support criticisms with evidence from the text or from other sources

Smith et al (J of Methodology, 2005, V3, pp 123) have shown that the analysis you use in Lines 241-250 is not the most appropriate for this situation. Please explain why you used this method.

Give specific suggestions on how to improve the manuscript

Your introduction needs more detail. I suggest that you improve the description at lines 57- 86 to provide more justification for your study (specifically, you should expand upon the knowledge gap being filled).

Comment on language and grammar issues

The English language should be improved to ensure that an international audience can clearly understand your text. Some examples where the language could be improved include lines 23, 77, 121, 128 – the current phrasing makes comprehension difficult. I suggest you have a colleague who is proficient in English and familiar with the subject matter review your manuscript, or contact a professional editing service.

Organize by importance of the issues, and number your points

1. Your most important issue
2. The next most important item
3. ...
4. The least important points

Please provide constructive criticism, and avoid personal opinions

I thank you for providing the raw data, however your supplemental files need more descriptive metadata identifiers to be useful to future readers. Although your results are compelling, the data analysis should be improved in the following ways: AA, BB, CC

Comment on strengths (as well as weaknesses) of the manuscript

I commend the authors for their extensive data set, compiled over many years of detailed fieldwork. In addition, the manuscript is clearly written in professional, unambiguous language. If there is a weakness, it is in the statistical analysis (as I have noted above) which should be improved upon before Acceptance.

A vertebra of a small species of *Pachycetus* from the North Sea and its inner structure compared with other basilosaurid vertebrae from the same site.

Henk Jan van Vliet ^{Corresp., 1}, Mark E.J. Bosselaers ^{2, 3}, Dirk K. Munsterman ⁴, Marcel Dijkshoorn ⁵, Jeffrey Joël de Groen ⁵, Klaas Post ⁶

¹ Altrecht, Utrecht, The Netherlands

² Koninklijk Belgisch Instituut voor Natuurwetenschappen, Brussel, Belgium

³ Koninklijk Zeeuwsch Genootschap der Wetenschappen, Middelburg, the Netherlands

⁴ Geological Survey of the Netherlands, Netherlands Organisation for Applied Scientific Research TNO, Utrecht, the Netherlands

⁵ Erasmus Universitair Medisch Centrum Rotterdam, Rotterdam, the Netherlands

⁶ Het Natuurhistorisch (Natural History Museum, Rotterdam), Rotterdam, The Netherlands

Corresponding Author: Henk Jan van Vliet
Email address: henkjanvanvliet@yahoo.com

A cetacean vertebral centrum, dredged from the tidal channel Het Scheur in the Western Scheldt Estuary, in proximity of the Belgian-Dutch border, is here described. In Het Scheur and nearby Wielingen, middle to late Eocene strata crop out at the current seafloor. The last decades vertebrae of at least three different large Eocene cetacean taxa have been discovered in this area, a diversity which is unparalleled in other European sites. The study vertebra has all characteristics of torso vertebrae of *Pachycetus* and belongs to a small species of this genus. In contrast to the other vertebrae, it was relatively dated by dinoflagellate cysts in adhering sediments. It is one of the very few remains of *Pachycetus* from Europe, which age could be assessed with reasonable certainty. The inner structure of the vertebral centrum and vertebral centra of several other basilosaurid taxa was studied by using high-quality CT scans. Notwithstanding differences in size, shape, inner structure and compactness, the architecture of basilosaurid vertebral centra appears to be basically similar. Also the inner vascularisation of the vertebral centrum has been studied and a remarkable pattern of five interconnected vascular systems is observed. The vascularisation of basilosaurid vertebrae, which have a thick, multi-layered cortex, differs significantly from what is seen in human vertebrae, which lack a comparable cortex.

A vertebra of a small species of *Pachycetus* from the North Sea and its inner structure compared with other basilosaurid vertebrae from the same site.

HENK JAN VAN VLIET¹, MARK BOSSELAERS^{2,3}, DIRK K. MUNSTERMAN⁴, MARCEL DIJKSHOORN⁵, JOËL DE GROEN⁵ AND KLAAS POST⁶

¹ Abel Tasmanstraat 41, 3531 Utrecht, the Netherlands

² Koninklijk Belgisch Instituut voor Natuurwetenschappen, Vautierstraat 29, 1000 Brussel, Belgium

³ Koninklijk Zeeuwsch Genootschap der Wetenschappen, Koudsteensedijk 7, 4331 JE Middelburg, the Netherlands

⁴ Netherlands Organisation for Applied Scientific Research TNO- Geological Survey of the Netherlands, Utrecht, P.O. Box 80015, 3508 TA Utrecht, the Netherlands

⁵ Erasmus Universitair Medisch Centrum Rotterdam, Dr. Molewaterplein 40, 3015 GD Rotterdam, the Netherlands

⁶ Het Natuurhistorisch (Natural History Museum, Rotterdam), Westzeedijk 345, 3015 AA Rotterdam, the Netherlands

Corresponding Author:

HENK JAN VAN VLIET

Abel Tasmanstraat 41, 3531 Utrecht, the Netherlands

Email address: henkjanvanvliet@yahoo.com

Abstract

A cetacean vertebral centrum, dredged from the tidal channel Het Scheur in the Western Scheldt Estuary, in proximity of the Belgian-Dutch border, is here described. In Het Scheur and nearby Wielingen, middle to late Eocene strata crop out at the current seafloor. The last decades vertebrae of at least three different large Eocene cetacean taxa have been discovered in this area, a diversity which is unparalleled in other European sites. The study vertebra has all characteristics of torso vertebrae of *Pachycetus* and belongs to a small species of this genus. In contrast to the other vertebrae, it was relatively dated by dinoflagellate cysts in adhering sediments. It is one of the very few remains of *Pachycetus* from Europe, which age could be assessed with reasonable certainty. The inner structure of the vertebral centrum and vertebral centra of several other basilosaurid taxa was studied by using high-quality CT scans. Notwithstanding differences in size, shape, inner structure and compactness, the architecture of basilosaurid vertebral centra appears to be basically similar. Also the inner vascularisation of the vertebral centrum has been studied and a remarkable pattern of five interconnected vascular systems is observed. The vascularisation of

basilosaurid vertebrae, which have a thick, multi-layered cortex, differs significantly from what is seen in human vertebrae, which lack a comparable cortex.

Introduction

In 1873 Brandt published a detailed description by Paulson regarding several archaeocete vertebrae from Ukraine (called *Zeuglodon rossicus* by Paulson) and changed this name to *Zeuglodon paulsonii* Brandt, 1873. Torso vertebrae of this taxon are quite characteristic, in being 1) large, 2) elongated, 3) in having a thick, multi-layered cortex, 4) a pock-marked surface, 5) elongated transverse processes, 6) elongated pedicles of the neural arch and 7) pachyostotic pedicles of the neural arch (Brandt, 1873; Gol'din & Zvonok, 2013). Later Kellogg (1936) changed the name to *Platyosphys paulsonii*. However, recently it became clear that in 1883 Van Beneden already erected the taxon *Pachycetus robustus* Van Beneden, 1883 based on a large vertebra (NsT90) and a large rib fragment (NsT92). The taxon occurred from the Bartonian to Priabonian successions in the Helmstedt region, Germany (Van Beneden, 1883; Van Vliet et al., 2020). Both fossils have similar characteristics in common with the vertebrae and ribs of *Platyosphys* from Ukraine. Hence, the genus name *Pachycetus* instead of '*Platyosphys*' was therefore proposed by Van Vliet et al. (2020). However, the species name *robustus* was restricted to NsT90 and NsT92 from the Helmstedt region. Apart from these large *Pachycetus* remains from Europe, two small species of *Pachycetus* were described during the last decades: *Pachycetus wardii* Uhen, 1999 from Bartonian strata of North Carolina (Uhen, 1999, 2001) and Virginia (Weems, 2011), and *Pachycetus aithai* Gingerich & Zouhri, 2015 from Bartonian sediments in Morocco. Recently, *P. aithai* was renamed to *Antaecetus aithai* and the subfamily Pachycetinae was erected for both the early basilosaurid genera *Pachycetus* and *Antaecetus* (Gingerich et al., 2022).

The vertebra NMR-16642 in this study is part of a collection of fourteen vertebrae and one neural arch which all show basilosaurid characteristics. The remains have been dredged from tidal channels Wielingen and Het Scheur in the Western Scheldt Estuary along the Belgian-Dutch border between 1996 and 2017. In these tidal channels Palaeogene successions crop out at the seafloor. Most vertebrae are from large taxa representing three morphotypes (Van Vliet et al., 2022). To date, thirteen vertebral centra and the partial neural arch of this collection have been described (Post, 2007; Schouten, 2011; Post & Reumer, 2016; Post et al. 2017; Van Vliet et al., 2022). Yet, another vertebral centrum had been dredged from Het Scheur which is assigned to a species of *Pachycetus*, Morphotype 1a in this publication. It is not-abraded and was still firmly embedded in sediments, which enabled dating by the age-diagnostic dinoflagellate cysts. Because it is maybe the first fossil of *Pachycetus* in Europe, from which age assessment was possible, it is described separately in this study. In addition,

its inner structure has been investigated with CT scans and is compared to the three vertebral morphotypes presently known from this site.

Geological setting

Marine Palaeogene strata are covered by relatively thin beds of Neogene sediments in the area of the tidal channels Wielingen and Het Scheur in the Western Scheldt Estuary near the Belgian-Dutch border (Fig. 1). These channels have been artificially deepened for navigation since the sixties of the last century and Palaeogene strata crop out at the seafloor (Van Vliet et al., 2022). At Wielingen, only the Priabonian Zelzate Formation, but at Het Scheur, located more to the west, also the Middle Eocene Maldegem Formation (Lutetian to Bartonian in age) is encountered, because the Palaeogene strata are tilted and dip to the northeast (Du Four et al. 2006; Post & Reumer, 2016). The Maldegem Formation consists of grey and blue-grey, fine silts and clay, reaching here a thickness of about 45 to 60 m (Du Four et al. 2006). Seven members are distinguished in the Maldegem Formation (Le Bot et al., 2003) of which the Onderdijke Member, consisting of blue-grey clays and the Buisputten Member, comprising sands are considered relevant for this study. Palaeogene sediments in Belgium show many hiatuses, indicative of transgressive and regressive phases (Vandenbergh 2004) (Fig. 2C).

Materials & Methods

The vertebral centrum NMR-16642 was dredged by commercial fishing vessel OD 31 in 2017. The vertebra is housed in the collections of Het Natuurhistorisch (the Natural History Museum Rotterdam, NMR) in the Netherlands. The specimens to which NMR-16642, Morphotype 1a is compared are: NMR-12331, NMR-12332, NMR-3404 (Morphotype 1b), NMR-10284 (Morphotype 2), NMR-10283 (Morphotype 3) from Wielingen/Het Scheur at the Belgian-Dutch border, all housed in the collections of Het Natuurhistorisch (the Natural History Museum Rotterdam, the Netherlands, as well as MSGB No. 25.191 from Taradell, Spain, housed in the collections of the Museo Geológico del Seminario de Barcelona in Spain. The vertebral centrum SMNS 10934b, from the Bartonian of Egypt has been studied in the Staatliches Museum für Naturkunde Stuttgart, Germany.

Palynological analysis—The age dating is not based on the vertebra NMR-16642, but on dinoflagellate cysts analysis of the adhering sediments. The accompanying sediment deposition is considered to be contemporaneous with the vertebra itself. Standard palynological techniques, including HCL and HF digestion, no oxidation and 15 µm sieving, were applied. The slides were mounted in glycerine jelly. Dinocyst taxonomy is according to that cited in the Lentin and Williams Index 2019 (Fensome et al., 2019). One microscope slide per sample was counted until a minimum of 200 palynomorphs (spores, pollen and dinoflagellate cysts) had been identified. The remainder of the slides were scanned for rare taxa. Miscellaneous fossils (like e.g. Pediastrum, Botryococcus)

were also counted, but kept outside the total sum of 200 specimens. The Miocene dinoflagellate cyst (dinocyst) zonation is based on Munsterman & Brinkhuis (2004), recalibrated to the Geological Time Scale of Ogg et al., 2016 (Munsterman et al., 2019). This zonation is based on consistent dinocyst events (on last and first occurrence datums: LOD and FOD) from available peer-reviewed palynological contributions in NW Europe and also includes the use of a global compilation calibrated to paleomagnetic, calcareous plankton and/or foraminifera/bolboforma (e.g. De Verteuil and Norris, 1996; Van Leeuwen, 2000; Zevenboom, 1995 and refs. herein). The age-assessments have been cross-validated by correlation to recognized sea-level fluctuations (Hardenbol et al., 1998; Munsterman & Brinkhuis, 2004).

Results of the palynological analysis—The palynological assemblage is relatively rich in marine dinoflagellate cysts. The variety of cysts is high (Fig. 3). Tasmanaceae (phrasinophyte algae associated with nutrient-rich, shallow marine conditions and stagnated ventilation) are also well presented. In Eocene strata Tasmanaceae are only commonly recorded in the Asse Clay Member (Dutch lithostratigraphical equivalent of the Maldegem Formation) from Zeeuws-Vlaanderen (e.g. Munsterman, 2003; Munsterman 2004). Reworking from a slightly older mid-Eocene, Lutetian stage is also recorded (e.g. by the presence of the dinocysts *Areosphaeridium ebdonii*, *Diphyes pseudoficusoides*, and *Rhombodinium rhomboideum*). A late Middle Eocene, Bartonian age is inferred by the FOD of *Rhombodinium draco* and the LOD's of *Rottnestia borussica* and *Areosphaeridium fenestratum*. dinocyst zone E7b, last part of NP16 to mid NP17 (Bujak & Mudge, 1996, Powell, 1992, and Gradstein et al., 2020). An origin from older strata, which have been eroded later, can ~~in our opinion~~ be excluded, as the vertebra does not show any signs of abrasion by sea currents or transport. The current dating is confirmed by the presence of *Cordosphaeridium funiculatum* (FOD in the Bartonian) (Fig. 3). Large hiatuses are present in the local section (Vandenberghe et al., 2004). Based on the results of the dinoflagellate cysts interpretation, the vertebra could originate from two members of the Maldegem Formation, the Onderdijke Member or the Buisputten Member 2. The latter consists of sand (see 'Geological setting'), the former of stiff clay with some silts and sands (Le Bot et al., 2003). The vertebra was embedded in clay and, being not-abraded, indicating an origin from the late Bartonian Onderdijke Member as considered most probable. Hence the age is approximately about 38 Ma (37.7- 38.6 Ma) (Fig. 4).

The relative length of a vertebral centrum is calculated by its dorsal anteroposterior length to anterior width ratio: $\text{relative length} = L_d/W_a$. Because the epiphyses are lacking in nearly all vertebral centra, the given relative length will be an underestimation. The relative width of a vertebral centrum is calculated by its anterior width to anterior height ratio: $\text{relative width} = W_a/H_a$.

CT scan—Scans were performed at the Department of Radiology and Nuclear Medicine, Erasmus Medical Center, Rotterdam, the Netherlands on a first generation photon-counting detector CT scanner (NAEOTOM Alpha, Siemens Healthineers). Photon-counting CT typically can generate CT images at higher spatial resolution compared to conventional energy integrating detector CT, while being able to scan larger objects than micro-CT. For this study 0.2 mm overlapping cross-sectional slices were acquired with the ultra-high resolution scan mode allowing a resolution up to 0.11 mm (in-plane). From the primary scan data axial, coronal and sagittal 2D CT images were generated. 3D images were reconstructed on a post processing server (Syngo VIA VB60, Siemens Healthineers) with a “cinematic rendering technique”. Cinematic rendering is a relative new technique for CT data which allows 3D images while maintaining sharpness and resolution, where the more commonly used “volume rendering technique” requires to smooth the 2D dataset with lower resolution reconstruction algorithms prior to 3D reformatting.

The reconstructions of the dorsoventral vascular system in vertebral centra of *Pachysetus* spp. have been made by a compilation of slices from these CT scans. These were 16 slices of vertebral centrum NMR-16642, each 1.9 mm thick; 37 slices from vertebral centrum NMR-12331, each 2.6 mm thick; 26 slices of NMR-12332, each 3.8 mm thick; 23 slices of NMR-3404, each 4.1 mm thick.

Terminology—The genus names ‘*Platyosphys*’ Kellogg, 1936 and ‘*Basilotritus*’ Gol’din & Zvonok, 2013 are replaced by *Pachysetus* Van Beneden, 1883 (Van Vliet et al., 2020). We follow Ratcliffe (1980), De Buffrénil et al., (1990), Houssaye et al., (2015) and Martínez-Cáceres et al., (2017), for anatomical and osteological terms.

Institutional abbreviations—FSAC Bouj, Faculté des Sciences Ain Chock, Boujdour collection, Université Hassan-II de Casablanca, Morocco; KOM, Kirovograd Oblast Museum, Ukraine; MGSB, Museo Geológico del Seminario de Barcelona, Spain; NCSM, North Carolina Museum of Natural Sciences, Raleigh, North Carolina, USA; NMR, het Natuurhistorisch, Rotterdam (Museum of Natural History, Rotterdam), the Netherlands; NsT (= MMG: NsT), Museum für Mineralogie und Geologie: Niedersachsen Tertiär, Senckenberg Naturhistorischen Sammlungen, Dresden SMNS, Staatliches Museum für Naturkunde in Stuttgart (State Museum of Natural History in Stuttgart)

Anatomical abbreviations — AEP, anterior external vertebral venous plexus; AIP, anterior internal vertebral venous plexus; anterolat equatorial art, anterolateral equatorial arteries; art, artery/arteries; AVB, anterior vertebral canal branch; Co.,

compactness; metaphyseal anast art, metaphyseal anastomosing artery; PIP, posterior internal venous vertebral plexus; Su, surface; VC, vascular canals.

Results

Systematic Paleontology

Order CETACEA Brisson, 1762

Suborder PELAGICETI Uhen, 2008

Family BASILOSAURIDAE Cope, 1868

Subfamily: PACHYCETINAE Gingerich, Amare & Zouhri, 2022

Genus PACHYCETUS Van Beneden, 1883

Material—One posterior thoracic vertebral centrum (NMR-16642). [Fig. 4](#); Table 1.

Description—Vertebral centrum with the transverse processes and the pedicles of the neural arch preserved. It is moderately elongated, with a length to width ratio of 1.10. The epiphyses are lacking, indicating that the specimen involved was not yet fully-grown. The width exceeds the height, with a width to height ratio of 1.26. The anterior epiphyseal side is more or less oval-shaped; the posterior epiphyseal side is trapezoid-shaped. The multi-layered cortex is thick. The dorsal surface has a prominent medial ridge, running over the entire length of the vertebra. Several small foramina appear to be present at the dorsal surface. There are no ventral foramina. The pedicles of the neural arch are elongated, pachyostotic and massive as are the transverse processes. The transverse processes are directed more or less horizontally and are located at about the midpart of the centrum. They are stocky and the projection is short. Laterally, they bear a deep, oval fovea for the tuberculum of the rib which is confluent with a shallow fovea for the capitulum of the rib, located somewhat more anteriorly on the transverse process. Like in *Antaetetus aithai*, the deep foveae have a pitted surface, suggestive of a cartilaginous or ligamentous articulation with the rib (Gingerich et al., 2022) (Fig. 4E). The ventral side of the corpus is broad, wide and more or less flat. It has three antero-posteriorly directed ridges: a medial one and two lateral ridges. The lateral ridges are running more or less oblique; they start anteriorly near the medial ridge and widen sidewise to the posterior corners of the vertebral body. Here, they have flat protuberances, resembling hemal processes in caudal vertebrae. An elongate, but shallow and small fossa is seen at both sides of the medial ridge. The centrum is not or only slightly permineralised, and it is not abraded. It is grey-brownish in colour. There are multiple drilling holes, made by marine organisms. For dimensions, see Table 1.

Comparison—The pachyostotic and elongated pedicles of the neural arch, and the antero-posterior elongation of the transverse processes of NMR-16642 are considered diagnostic for Pachycetinae (Kellogg, 1936; Gol'din & Zvonok, 2013; Gingerich & Zouhri, 2015; Van Vliet et al., 2020). Because of the lateral foveae and the articulation

pits for the ribs, NMR-16642 is considered a thoracic vertebra and the elongation points to a posterior position. More anteriorly positioned thoracic vertebrae are less elongated and have a smooth ventral side (Van Vliet et al., 2020). The grooves and ridges at the ventral side of NMR-16642 are similar to a presumably posterior thoracic vertebral centrum (NsT90) of *Pachycetus robustus* from Germany (Van Vliet et al., 2020) (Fig. 6A1-B1). However, NMR-16642 is smaller in size than NsT90, although the latter also represents a not fully-grown individual (Fig. 6). NMR-16642 is also significantly smaller than the large species of *Pachycetus* known from Ukraine (Kellogg, 1936: table 24, 25), Germany (Uhen & Berndt, 2008; Van Vliet et al., 2020; Gingerich et al., 2022) and from Belgium (Van Vliet et al., 2022). The dimensions of NMR-16642 equal those of the posterior-most thoracic vertebrae of *Pachycetus wardii* Uhen, 1999 (missing one or two epiphyses, see Uhen, 2001) from North Carolina, or *Antaecetus aithai* Gingerich & Zouhri, 2015 from Morocco.

Comparison of axial sections of NMR-16642 with those of NMR-12332, assigned to a large species of *Pachycetus*, shows that the former falls completely within the innermost cortical boundaries of the latter (Fig. 7). Both have a thick, multi-layered cortex. It is not conceivable that NMR-16642 represents an ontogenetic very young individual of the large *Pachycetus* species, which vertebrae would become as large as NMR-12332 during the individual's maturation. Increasing in size implies the deposition of ever more cortical bone layers and the internal morphological structure of NMR-16642 would be finally very different from that of NMR-12332, unless extensive and complete remodelling of the innermost cortical layers would have taken place. No sign of this is noted in NMR-12332, in which the inner border of the multi-layered cortex is rather sharply delineated from the spongy-like (A-B) or spongy (C) bone underneath (see 'Inner structure, cortex' and 'Vascularisation, endocortical VC'). Obviously, the vertebrae, the small (NMR-16642) and the large (NMR-12332), represent two different species of *Pachycetus*. See Fig. 8 and Table 2 for a comparison of the dimensions between posterior-most thoracic vertebrae, assigned to small and large species of *Pachycetus*.

Inner structure

Cortex and spongiosa—The cortex of NMR-16642 consists of a thin, compact outer part and a thick, spongy-like, multi-layered inner part, both consisting of periosteal bone (Fig. 9). The multi-layered part of the cortex is considered to be lamellar-zonal bone (*sensu* De Buffrénil et al., 1990), with abundant vascular canals (see 'Discussion'). At the axial midpart of NMR-16642, the thin outer part is about 0.75 to 2.5 mm thick. The multi-layered inner part is maximum 17 to 20 mm thick in this section ('1' in Fig. 9A2). Beneath the multi-layered cortex, also spongy-like bone with a more chaotic architecture is present, which is considered to be also periosteal bone, but without layers. It is most prominent at the vertebra's midpart and within the transverse processes ('2' in Fig. 9A2, B2, C2). Two conical structures, constituting a large part of the inner structure of the vertebral centrum, consist of a seemingly amorphous spongy bone (see 'Discussion' for the osteogenic dynamics) ('3' in Fig. 9 B2, C2). The top of the two

coni meet each other at the vertebral midpart; they are not visible in the axial section of the vertebral midpart (Fig. 9A).

The compactness has been measured in two axial sections; the first one through the midpart of the vertebra and the second one through the anterior conus. In both sections, the compactness of the cortex (outer part and looser multi-layered part underneath) is higher than that of the central parts. The highest cortical compactness is seen at the lateral side of the vertebral centrum, near the outer part of the transverse process, and at the ventral side.(about 0.84). At these places the vertebra can be called osteosclerotic (De Buffrénil et al., 2010). The compactness of the cortex is ventrally and dorsally somewhat lower. The compactness of the (anterior) conus is higher, than that of the vertebral axial midpart. In both sections, the central part of the vertebra has the lowest compactness with values at the midpart of the vertebra as low as 0.40. The compactness of the axial midpart of the thoracic vertebra NMR-16642 is rather similar to that of the axial midpart of a caudal vertebra from Taradell, Spain, MSGB No. 25.191, also assigned to a small species of *Pachycetus* (Van Vliet et al., 2023). The total compactness of the axial midpart of NMR-16642 is 0.61, that of the Taradell vertebra 0.56. The compactness of the multi-layered cortex of MSGB No. 25.191 is only slightly lower than that of NMR-16642 (0.53-0.58, resp. 0.68-0.69), whereas the compactness of the central part of MSGB No. 25.191 is slightly higher (0.55 resp. 0.50) (Table 3; Fig. 10).

Comparison

The inner architecture of the vertebral centrum NMR-16442, Morphotype 1a is compared to vertebral centra from Het Scheur at the Belgian-Dutch border, in which three different basilosaurid morphotypes are recognised. These are: Morphotype 1b, elongated (torso) vertebrae (in which the length significantly exceeds the width), which are represented by the posterior thoracic vertebral centra NMR-12331 and NMR-12332, as well as the lumbar vertebral centrum NMR-3404, all ascribed to a large species of *Pachycetus*. The large vertebral centrum of *Basilosaurus cetoides* Owen, 1839, USNM 510831, is added to these in Fig. 11, but the latter is here not investigated in detail.

Morphotype 2, not-elongated (torso) vertebrae (in which the length equals the width), which is represented by the large posterior thoracic or lumbar vertebral centrum, NMR-10284, an indeterminable basilosaurid (Fig. 12A).

Morphotype 3, 'shortened' (torso) vertebrae (in which the length is significantly smaller than the width) which is represented by the caudal vertebral centrum NMR-10283, apparently a new taxon, not comparable to any of the known basilosaurid genera (Fig. 12B & Table 3).

Microstructure

Cortex—Elongated vertebrae of Morphotype 1. The multi-layered cortex in the vertebrae of *Pachycetus* and *Basilosaurus* is ventrally much thicker than dorsally (Fig. 11). The cortex in the small vertebra NMR-16642, consisting of a rather loose spongy-like bone, clearly differs from the very compact cortex seen in vertebrae of the large species of *Pachycetus* sp. (NMR-12331, NMR-12332 and NMR-3404). The layering in the outer part of the cortex is here hardly visible. However, the inner layers consist of spongy-like bone. Except for the greater compactness of the cortex, the axial section of the midpart of NMR-3404 (Fig. 11C) is more or less similar to that of NMR-16642 (Fig. 9A2). The cortex is divided into two parts: a very compact one (1a) and a less compact one (1b). The transition between the two parts is more or less fluent, whereas the transition to the amorphous inner part is rather sharply delineated. Davydenko et al. (2023: p. 5) discerned three parts: a compact outer part, a transition zone and a less compact inner part. The cortex of the vertebral centrum of *Basilosaurus cetoides*, USNM510831 resembles more that of the NMR-10284, Morphotype 2 (Fig. 11D), having alternating compact and spongy-like layers (Fig. 12).

Not-elongated vertebrae of Morphotype 2. The large vertebral centrum NMR-10284 has a thick multi-layered cortex, which is dorsally much thicker, than seen in the elongated vertebral centra of Morphotype 1a-b. The cortex differs from that of the large *Pachycetus*, consisting of spongy-like and compact layers (see below). At the left ventral side, the cortex is broken off through a spongy, looser layer along a compact layer underneath, a phenomenon in archaeocete vertebrae which was already observed by Müller (1849).

‘Shortened’ vertebrae of Morphotype 3. Although the vertebra NMR-10639 is large, it seemingly consists entirely of spongy-like bone, except for a thin outer cortex. The layering of the thick, inner cortex is not clearly visible at most places, because of the loose structure. The cortex is dorsally only slightly thinner than ventrally (Fig. 12).

Conus—All here described vertebral centra appear to have two coni (Fig. 13; Table 2). Morphotype 1. The coni of NMR-16642 consist of spongy bone (with occasionally a vascular canal going straight to the epiphyseal end (Figs 12A, 13A). (see also ‘discussion’). The coni in vertebrae of the large *Pachycetus* sp. (NMR-12331, NMR-3404) consist of a far more compact bone, also pierced by some vascular canals. It appears however to be more radiolucent than the radio-opaque cortex, being grey instead of clear white on the CT scans (Figs 12B-C, 13B). A remarkable phenomenon is observed in the vertebral centra of both the small and large species of *Pachycetus* (Fig. 14A-B) and to a lesser extent also in those of morphotypes 2 and 3 (Fig. 14C-D): the coni appear to be layered. This layering is in a plane parallel to the epiphyseal sides.

Obviously they indicate a not-continuous growth with periods of **dense** and less dense bone depositions, probably reflecting differences in growth rate.

Morphotype 2. The coni in the vertebral centrum NMR-10284 consist of a less compact spongy bone with more trabeculae and vascular canals, than seen in vertebrae of the *Pachycetus* sp.

Morphotype 3. Notwithstanding the loose structure of the large NMR-10283, there are two coni, which are rather flat. (Fig. 13F).

Vascularisation. Five main vascular systems are discerned in NMR-16642, which are also present in the three morphotypes of investigated vertebrae. These are 1) a system of midvertebral dorsal (and, if present ventral) vascular canals (the midvertebral VC), 2) a system of vascular canals surrounding the two coni, here called the epiconal vascular canals (epiconal VC), 3) a system of vascular canals within the two coni, here called the endoconal vascular canals, 4) a system of tiny vascular canals in the inner layers of the cortex, here called the endocortical vascular canals (endocortical VC) and 5) the apparently randomly scattered tiny vascular canals, here called the accessory vascular canals (accessory VC). The midvertebral VC and the epiconal VC are directly connected to a central node at the vertebra's midpart, here called the central vascular node. The vascularisation of the epiphyseal discs has not been studied as most vertebrae are lacking the epiphyses.

The midvertebral VC—Near the dorsal surface of vertebral centrum NMR-16642, six foramina are discerned, orifices of vascular canals. There is one central vascular canal, going in a more or less straight axial plane from a central vascular node at the midpart of the vertebral centrum to the dorsal surface, bending slightly posteriorly toward the left side of the median ridge. Its width varies between about 8 mm at the dorsal surface to 4.5 mm at the central vascular node. Its counterpart on the right side is at least partly obliterated, which is probably an anomaly (Fig. 11A1). The five other vascular canals are about 3 to 4 mm in width. Three of these are bending posteriorly toward the right side of the median ridge. One of these is a branch of the open left central canal and splits near the dorsal surface of the vertebra into two canals. The third vascular canal arises from an epiconal canal (see below). Possibly the presence of these three canals at the right side, none of which with a left counterpart, is due to the obliteration of the right central vascular canal. Anterior to the open central canal, a vascular canal is running from the central vascular node to the dorsal surface, bending anteriorly and splitting into two canals which open to the left and right side of the median ridge (Fig. 15A). NMR-16642 lacks ventral vascular canals or foramina.

The midvertebral VC in NMR-16642 is compared to that in the posterior thoracic vertebral centra NMR-12331 and NMR-12332, and the lumbar vertebral centrum NMR-

3404 of the large *Pachycetus* sp. Contrary to the NMR-16642, in these three vertebrae, ventral vascular canals are present, which could be ascribed to a more posterior position in the vertebral column.

NMR-12331 has two main dorsal central canals, about 2 to 6 mm in width, going through the vertebra's midpart. At the dorsal surface these two canals become much larger, both ending in separate fossa's (left: 95 mm; right: 63 mm in length). Two other canals are present. A tiny one is going from the central vascular node in a straight line to the dorsal surface. The other canal, does not go through the central vascular node, but arises more dorsally from the epiconal system, ending in the left dorsal canal. There are four ventral vascular canals, a left-right anterior and a left-right posterior pair. These are about 1.5 to 9.0 mm in width. They are not going in a straight plane to the ventral surface, but follow the course of the ventral part of the epiconal VC, each ending in a separate narrow fossa of about 50 mm in length. In fact, they seem to be enlarged epiconal canals (Fig. 15B).

NMR-12332 has two main dorsal central vascular canals, about 4 to 7 mm in width, going through the vertebra's midpart. At the dorsal surface these canals increase in size, both ending in a separate fossa (left: 50 mm; right: 65 mm in length). The central canals are accompanied by several canals, bending more posteriorly and anteriorly. The canals all end in the central vascular node. Ventrally, two vascular canals are present. The left one is about 2 mm in width, ending in a small ventral fossa, about 15 mm in length. The right one splits into four tiny canals, each about 1.0 to 1.5 mm in width, ending in in a ventral fossa about 13 mm in length (Fig. 15C).

NMR-3403 has only two dorsal central vascular canals (each slightly more than 11 mm in width), without accompanying smaller canals. Both becoming larger toward the dorsal surface and ending in separate dorsal fossae (left: 61 mm; right: 56 mm in length). They go ventrally through the vertebra's midpart (about 11.5 mm at the central vascular node). There is a large ventral vascular canal lying at the left side, that splits into a posterior (about 7.5 mm in width) and an anterior branch (about 9 mm in width). The anterior branch immediately splits into a left and a right canal (9 resp. 7 mm in width), fusing again near the ventral surface. The left vascular canal is larger than the right one. Both become larger toward the ventral surface, ending in two separate ventral fossae (left: 58 mm; right: 28 mm in length) of the vertebral centrum (Fig. 15D; Table 2).

The other four main vascular systems (the epiconal VC, endoconal VC, endocortical VC and accessory VC), as seen in NMR-16642, are compared with the vertebral centra of the three morphotypes of basilosaurid vertebral centra.

The epiconal VC—On the surface of the conus in the investigated vertebrae, a peculiar pattern of vascular canals is present ~~is present~~ at more or less regular places, resembling the ribs of an umbrella. They are clearly seen on an isolated conus of the large *Pachycetus* sp., ID 20-4 from the Helmstedt region, Germany, as well as in a

vertebral fragment of *Pachycetus* sp., SMNS 10934b, from the Bartonian of Egypt (Fig. 16). The epiconal VC are schematically indicated in Fig. 15). Also the two coni in NMR-16642 are surrounded by about 20-30 canals of the epiconal VC; some of these canals are rather large, being more than 2.3 mm in diameter (Fig. 17A2) They originate from the central vascular node and are running to the epiphyseal side of the vertebrae. Here they pierce the multi-layered cortex near the epiphyseal sides, crossing the vascularised inner layers of the cortex. The epiconal VC is also present in the large species of *Pachycetus* (NMR-12331) (Fig. 17B). It was earlier briefly described and figured by Van Vliet et al., (2020: p. 129 & fig. 3b1, 3); Van Vliet et al., (2022: p. 21 & fig 14f) in large species of *Pachycetus* and it is probably this vascular system that was described and figured by Davydenko et al. (2023: p. 3 & fig. 1b) as 'radial vascular canals'. The vascular system is also present in the other two types of basilosaurid vertebral centra (Fig. 18). The canals are about 0.5 to more than 1.5 mm in diameter.

The endoconal VC—Rather than amorphous, the coni appear to contain multiple vascular canals going in a straight way toward the epiphyseal sides. They are branches of the epiconal VC (Figs 14, 16, 18). Here they end between the radiating ridges of the vertebral side of the epiphyseal discs. In the here investigated basilosaurid taxa, the coni differ from each other apart in having a more compact or a more loose inner structure and in having smaller or larger endoconal canals (Fig. 19).

The endocortical VC—Another vascular system is constituted by several layers with multiple tiny blood vessels, present in the inner layers of the cortex. They are running ventrally and laterally in a anteroposterior direction (Fig. 20), but at the transverse processes, the main direction is toward the tip of the transverse process (Fig. 21). The canals are maximum about 1.5 mm, but mostly less than 1 mm in diameter at the vertebral midpart and are decreasing in diameter near the epiphyseal sides. The innermost layer with multiple vascular canals appears to be rather sharply delineated from the amorphous inner part in especially the morphotypes 1a, 1b and 2 (Fig. 11A-C; Fig. 20A-C). These vascular systems are observed in all the three morphotypes of vertebral centra.

The accessory VC— In addition to these systems, also multiple, mostly tiny vascular canals are seen, which arise from the surface and are running toward the vascular node (Fig. 22). These are however hardly or not discernible in NMR-16642, Morphotype 1a, probably due to their small size and the spongy-like structure of the cortex. They are however clearly seen in the ventral side of the compact cortex of NMR-12331, Morphotype 1b, and appear to be abundant in NMR-10284, Morphotype 2. Also some of these canals are visible in NMR-10283 Morphotype 3. They differ from the epiconal VC in running in a straight line and in not being curved around the conus.

Discussion

Microstructure of bone—The architecture of the investigated vertebral centra is basically

similar to each other, regardless of being elongated, not-elongated or 'shortened', or of having a high or low compactness. Two coni, tapering toward the midpart of the vertebra, are surrounded by a multi-layered cortex, which is thickest at the midpart of the centrum. Vertebrae of *Basilosaurus cetoides* (not investigated in this study) seem to fall outside this general pattern, as the coni are remarkably obtuse and resemble cylinders (Gingerich et al., 2022). In the three morphotypes, the architecture is obviously a result of the dynamics of osteogenic processes. Like in all mammals, two types of bone are discerned: periosteal bone, deposited by the periosteum and giving rise to the cortex, and endochondral bone, deposited by the secondary growth centra at the epiphyseal discs and giving rise to the coni. Generally, both types of bone can be replaced and remodelled to spongy bone (De Buffrénil et al., 1990).

Similar as in archaeocete ribs (Gray et al., 2007), in the here investigated basilosaurid vertebrae the multi-layered vertebral cortex consists of periosteal, cyclical bone depositions (lamellar-zonal bone *sensu* De Buffrénil et al., (1990). At the primary growth centrum in the midpart of the vertebral centra the most periosteal layers have been deposited and the multi-layered cortex is thickest. This is readily seen in Fig. 13. Toward the epiphyseal sides of the vertebrae, less and less periosteal bone layers have been deposited, because here bone deposition occurred later in the individual's ontogenetic age. Remodelling and restructuring of bone with the appearance of secondary osteons, was seen in thin sections of the inner cortical layers regarding vertebrae, NMNH-P Ngr-12, of a large species of *Pachycetus*, ('*Basilotritus*') sp., from Ukraine (Davydenko et al., 2023). However, in the here investigated vertebrae (NMR-12331, NMR-12332, NMR-3404), Morphotype 1a, of a large species of *Pachycetus*, the persisting layering in the inner parts of the cortex indicates that remodelling of periosteal bone was not complete, but at least reduced, similar to what is observed in ribs of *Basilosaurus cetoides* or *Zygorhiza kochii* (De Buffrénil et al., 1990). The inner layers of the vertebral cortex in NMR-12331, NMR-12332 and NMR-3404 contain multiple vascular canals, which was also described by Davydenko et al. (2023) regarding NMNH-P Ngr-12. It reflects what is seen in ribs of *Basilosaurus cetoides* (De Buffrénil et al., 1990, fig. 3a). In vertebra NMR-16642, Morphotype 1a, of the small species of *Pachycetus*, the entire multi-layered cortex seems to have been replaced by spongy-like bone, but the original layering is still present. As complete remodelling and replacement of periosteal bone by trabecular bone cannot take place without destroying the layered architecture, the multiple cavities therefore are interpreted as vascular canals. The presence of multiple vascular canals in the outer layers of the cortex was also described by Van Vliet et al. (2023) regarding vertebra MG SB No. 25.191 of a small species of *Pachycetus* from Taradell, Spain. The cavities in alternating layers of loose, spongy-like and compact bone in the cortex of vertebrae of Morphotype 2, are interpreted as vascular canals too, because complete remodelling and restructuring of

compact bone to spongy bone by the endosteum in layers with a more loose structure did not take place in compact cortical layers underneath.

The conical processes obviously have been deposited by the secondary growth centres at the epiphyseal disc and the sigmoid-shaped outlines of the conical processes reflect the at first rapid, and later on decelerating growth rate in diameter of the epiphyseal disc. Being deposited by the secondary growth centres, they consist of endochondral bone. The amorphous bone underneath the cortex, surrounding the conical processes and present in the transverse processes, in the here investigated vertebrae is clearly different from the spongy bone of the conical processes (Fig. 9B2 & C2). The position of the endoconal VC seems to be fixed in the conus, because the canals are running from where they split off from the periconal canals, in a straight line to the epiphyseal side. Apparently the endoconal canals maintained their position, while growing in length with the vertebral centrum. The layering of the spongy bone in the conical processes (Figs 13A-B), parallel to the epiphyseal ends as seen in both the small and large species of *Pachycetus*, suggests that the spongy bone of the conical processes underwent an only moderate remodelling, contrary to bones in most mammals (De Buffrénil et al., 1990). In both the Morphotypes 2 and 3, mostly only some lines parallel to the epiphyseal side are seen, which are probably remnants of layers of more compact spongy bone (Fig. 14C-D). These are suggestive that resorption and remodelling of bone was more pronounced than in *Pachycetus* spp. Investigation of the microscopic bone structure will be necessary to confirm this.

In the large species of *Pachycetus* the outer surface of the conical processes is rather well delineated from the surrounding compact layers of the cortex and conical processes can easily become detached from the vertebral centrum (Van Vliet et al., 2020). Contrary to what is seen in scans of the large species of *Pachycetus* (NMR-12331, NMR-12332, NMR-3404), the compactness of the multi-layered cortex of NMR-16642 is not much higher than that of the conus (Fig. 10; Table 2) The same is observed in the caudal vertebra MSGB No. 25.191 from Taradell, Spain (Van Vliet et al., 2023). Because breakage occurs preferably along a layer of compact bone (see remark about NMR-10284, section 'Microstructure of the bone, cortex'), it is not probable that the conical processes of these two vertebrae of *Pachycetus* can be easily detached from the vertebral centrum. In this respect these vertebral centres seem to differ from *Antaecetus aithai*, as isolated conical processes of this taxon have been described by Gingerich & Zouhri (2015). Maybe this points to a higher cortical compactness in vertebrae of *Antaecetus aithai* from Morocco, which could suggest that the European small species of *Pachycetus* and *A. aithai* from Morocco represent different taxa.

Vascularisation—Blood supply to the central vascular node at the primary growth centrum was provided by the midvertebral VC, and probably also by the accessory VC.

This vascular node gave in its turn rise to the two umbrella-like epiconal VC. They surround the conus (Fig. 16) and, like these, became longer during growth. The epiconal VC gave rise to the endoconal VC and added to the blood supply of the epiphyseal ends from the inner side of the vertebral centrum (Fig. 17). By crossing the inner layers of the cortex (Fig. 18), they were connected to the endocortical VC. It is presumably especially the orifices of the accessory VC, as well as those of the epiconal VC near the epiphyseal sides, that can be seen as pock marks on the vertebra's surface.

Comparison—By lack of relevant literature about the vertebral vascularisation of **terrestrial mammals**, we had to refrain to **human vertebrae**. These obviously lack a thick, multi-layered cortex, and the vascularisation clearly differs from what is seen in basilosaurids. Three planes with arteries are present, more or less parallel to the epiphyses, arising from extraosseous arteries ([Ratcliffe, 1980](#)).

Midvertebral and metaphyseal planes—At the equatorial plane the so-called nutrient and two to four anterolateral equatorial arteries are present. Branches of these arteries go upward and downward to the epiphyseal sides. Both above and below, another plane with the so-called metaphyseal arteries are present. Following at first a straight course in the vertebral centrum, they split near their end in the centrum into coiled branches. Contrary to the equatorial and nutrient arteries, branches of the metaphyseal arteries go either upward (from the plane above the equatorial plane), or downward (from the plane under the equatorial plane) toward the epiphyseal sides and are oriented centrifugally. The periphery of the vertebral centrum is supplied by short peripheral arteries ([Ratcliffe, 1980](#)). Internal vertebral venous plexuses drain into external venous plexuses outside the vertebral centrum ([Moore et al., 2014](#)) (Fig. 23)

In human lumbar vertebral centra blood supply is directly from extraosseous arteries, whereas in basilosaurids blood supply from outside probably was going via the central vascular node. Separate equatorial arteries and separate planes with metaphyseal arteries are lacking in basilosaurid vertebrae. On the other hand there are similarities too. The nutrient arteries in human vertebrae are analogue with the dorsal arteries of the midvertebral VC in basilosaurids. There are about 10-20 intervertebral metaphyseal arteries in human vertebra, positioned in a ring above and below the vertebra's midpart, splitting into branches and centrifugally run to the epiphyses ([Ratcliffe, 1980](#)). These are reminiscent of the basilosaurid intervertebral epiconal VC, also positioned in a ring and oriented centrifugally to the epiphyseal sides. Blood supply of the periphery of human vertebral centra is provided by peripheral arteries, which are maybe analogue with the accessory VC, arising from the vertebral surface in basilosaurids. The vascular systems in basilosaurid vertebrae could perhaps be ascribed to the persistence of a non-remodelled periosteal, multi-layered cortex.

Conclusions

The vertebral centrum, NMR-16642 dredged from the Western Scheldt Estuary at approximately the Belgian-Dutch border in 2017, originated from the late Middle Eocene (Bartonian) Maldegem Formation (Belgian Nomenclature), which subaqueously crops out in the artificially deepened tidal channel Het Scheur, Belgium, and it most probably has been derived from the Onderdijk Member. It is, based on the microfossil content of the adhering sediments, ca. 38 Ma in age.

Comparison of CT scan images of the vertebral centrum with vertebrae of other basilosaurid taxa, revealed that their architecture is basically similar, consisting of a multi-layered cortex surrounding two con. Contrary to earlier observations, the presence of a thick, multi-layered cortex in the vertebral midpart of *Basilosaurus* is not an exception, but the common condition in the here investigated basilosaurid vertebrae.

Apart from the not-investigated blood supply of the epiphyses, five vascular interconnecting systems are discerned within the basilosaurid vertebral centra. Comparison with the vascularisation of human vertebral centra revealed different vascular systems, although also some similarities could be observed. The persistence of a cortex of periosteal bone with reduced remodelling and a probably only moderately remodelled spongiosa could explain the peculiar vascular systems within basilosaurid vertebrae.

Acknowledgements

We are grateful to Drs. Bram Langeveld, curator of Het Natuurhistorisch (Natural History Museum, Rotterdam), the Netherlands, who welcomed us always in a very friendly way and gave us ample opportunity to study the vertebral centra from Wielingen/Het Scheur. Also Dr. Eli Amson was very helpful, when we visited the Staatliches Museum für Naturkunde Stuttgart, Germany. Dr. Mark Uhen very kindly gave us a second opinion regarding vertebrae NMR-16642. Last but not least, Dr. Olivier Lambert was helpful with comments regarding the vertebra NMR-16642.

References

- Brandt JF. 1873. Untersuchungen über die fossilen und subfossilen Cetaceen Europas. *Mémoires de l'Académie impériale des Sciences de Saint-Pétersbourg*, VII^e série, tome XX: 1-372.
- Brisson MJ. 1762. *Regnum animale in classes IX. distributum, sive synopsis methodica sistens generalem animalium distributionem in classes IX, & duarum primarum*

- classium, quadrupedum scilicet & cetaceorum, particularem divisionem in ordines, sectiones, genera & species. Cum brevi cuiusque speciei descriptione, citationibus auctorum de iis tractantium, nominibus eis ab ipsis & nationibus impositis, nominibusque vulgaribus. Editio altera auctior.* Lugduni Batavorum: apud Theodorum Haak. 1-296
- Bujak J, Mudge D. 1994. A high-resolution North Sea Eocene dinocyst zonation. *Journal of the Geological Society, London* 151:449-462.
- Cope ED. 1868. An addition to the vertebrate fauna of the Miocene period, with a synopsis of the extinct Cetacea of the United states. *Proceedings of the Academy of Natural Sciences of Philadelphia* 19:138-156.
- Davydenko, S, Tretiakov, R, Gol'din, P. 2023. Diverse bone microanatomy in cetaceans from the Eocene of Ukraine further documents early adaptations to fully aquatic lifestyle. *Frontiers in Earth Science*: 1-12 DOI:10.3389/feart.2023.1168681
- De Buffrénil V, Ricqlès A, Ray CE, Domning DP. 1990. Bone histology of the ribs of the archaeocetes (Mammalia: Cetacea). *Journal of Vertebrate Paleontology* 10:455-466.
- De Buffrénil V, Canoville A, d'Anastasio R, Domning DP. 2010. Evolution of sirenian pachyosteosclerosis, a model-case for the study of bone structure in aquatic tetrapods. *Journal of Mammalian Evolution* 17:101-120.
- De Smet D, Martens K, DeBreuck W. 1997. Optimalisering van het opslaan en verwerken van gegevens van de watervoerende lagen met het oog op de uitwerking van een efficiënt grondwaterbeleid. *Laboratorium voor Toegepaste Geologie en Hydrogeologie, Geologisch Instituut Gent, project nummer TGO 94/47.*
- De Verteuil L, Norris G. 1996. Miocene dinoflagellate stratigraphy and systematics of Maryland and Virginia. *Micropaleontology, Supplement*. 42: 1-172.
- Du Four I, Schelfaut K, Vanheteren S, Van Dijk T. Van Lancker VRM. 2006. Geologie en sedimentologie van het Westerscheldemondingsgebied. In: Coosen, J. et al. (eds.) Studiedag: de Vlakte van de Raan van onder het stof gehaald, Oostende. *VLIZ Special Publication* 35:16-29.
- Eldrett JS, Harding IC, Firth JV, Roberts AP. 2004. Magnetostratigraphic calibration of Eocene-Oligocene dinoflagellate cyst biostratigraphy from the Norwegian-Greenland Sea. *Marine Geology* 204:91-127.

- Fensome RA, Williams GL, MacRae RA. 2019. Lentin and Williams index of fossil dinoflagellates. *AASP Contribution series*, 50: 1173 pp.
- Gingerich PD, Zouhri S. 2015. New fauna of archaeocete whales (Mammalia, Cetacea) from the Bartonian middle Eocene of southern Morocco. *Journal of African Earth Sciences* 111: 273-286.
- Gingerich PD, Amame A, Zouhri S. 2022. Skull and partial skeleton of a new pachycetina genus (Cetacea, Basilosauridae) from the Aridal Formation, Bartonian, middle Eocene, of southwestern Morocco. *PLoS ONE*. DOI.org/10.1371/journal.pone.0276110
- Gol'din PE, Zvonok EA. 2013. *Basilotritus uheni*, a new cetacean (Cetacea, Basilosauridae) from the late middle Eocene of eastern Europe. *Journal of Paleontology* 87: 254-268.
- Gradstein FM, Ogg JG, Schmitz MD, Ogg GM. *Geologic Time Scale 2020*. First edition. Elsevier. 1390 pages.
- Gray NM, Kainec K, Madar S, Tomko L, Wolfe S. 2007. Sink or swim? Bone density as mechanism for buoyancy control in early cetaceans. *Anatomical Record* 290:638-653 DOI:10.1002/ar.20533.
- Hardenbol J, Thierry J, Farley MB, Jacquin Th, De Graciansky PCH, Vail PR. 1998. Mesozoic and Cenozoic sequence chronostratigraphic framework of European Basins, Mesozoic and Cenozoic sequence chronostratigraphic chart 1, In: *Graciansky PCH, Hardenbol J, Jacquin Th, Vail PR*.
- Houssaye A, Tafforeau P, de Muizon C, Gingerich PD. 2015. Transition of Eocene whales from land to sea: Evidence from bone microstructure. *PLoS ONE*: 1-28 DOI:10.1371/journal.pone.0118409.
- Jayaraman MV. 2008. Preoperative and therapeutic endovascular approaches for spinal tumors. In: Kim, DH, Chang U, Kim S, eds *Tumors of the spine*, Philadelphia: Saunders, 327-339.
- Kellogg R. 1936. *A review of the Archaeoceti*. Carnegie Institution of Washington. 366 pp.

- Le Bot, S., Van Lancker, V., Deleu, S., De Batist, M. & Henriët, J.P. 2003. Tertiary and quaternary geology of the Belgian Continental Shelf. *Science Policy Office, Brussels, Belgium*. 75 pages.
- Linnaeus C. 1758. *Systema naturae per regna tria naturae, secundum classes, ordines, genera, species, cum characteribus, differentiis, synonymis, locis*. Tomus I. Editio decima, reformata, L. Salvii. 824 pp.
- Martínez-Cacéres, M. & de Muizon, C. 2011. A new basilosaurid (Cetacea, Pelagiceti) from the Late Eocene to Early Oligocene Otuma Formation of Peru. *Comptes Rendus Palevol* 10: 517-526.
- Moore KW, Dalley AF, Agur AMR. 2014. Clinically oriented anatomy. *Wolters Kluwers/ Lippincott Williams & Wilkins*. 7th edition. 1134 pp.
- Müller J. 1849. *Über die fossilen Reste der Zeuglodonten von Nordamerika, mit Rücksicht auf die europäischen Reste aus dieser Familie*. 38 pp. G. Reimer, Berlin.
- Munsterman DK. 2003. De resultaten van het dinoflagellaten onderzoek naar de ouderdom en het afzettingsmilieu van de boringen 55A0364 (Hulst), 54F0093 (Axel) en 48E0224 ('s Heer-Arendskerke). *TNO-NITG* 03-061-B, 20 pp.
- Munsterman DK. 2004. De resultaten van het dinoflagellaten onderzoek naar de ouderdom en het afzettingsmilieu van de boringen 54B0085 (Biervliet) en 54F0097 (Axel). *TNO-NITG* 04-016-B: 14 pp.
- Munsterman DK, Brinkhuis, H. 2004: A southern North Sea Miocene dinoflagellate cyst zonation. *Netherlands Journal of Geosciences*, 83 (4): 267-285.
- Munsterman DK, Ten Veen JH, Menkovic A, Deckers J, Witmans N, Verhaegen J, Kerstholt-Boegehold SJ, Van de Ven T, Busschers FS. 2019. An updated and revised stratigraphic framework for the Miocene and earliest Pliocene strata of the Roer Valley Graben and adjacent blocks. *Netherlands Journal of Geosciences*, 98, e8. <https://doi.org/10.1017/njg.2019.10>.
- Ogg JG, Ogg G, Gradstein, FM, 2016. A Concise Geologic Time Scale, pp. 240.
- Owen R. 1839. Observations on the Basilosaurus of dr. Harlan (*Zeuglodon cetoides*). *Transactions of the Geological Society of London* 6: 69-79. DOI:[10.1144/transgs1b.6.1.69](https://doi.org/10.1144/transgs1b.6.1.69)

- Post K. 2007. Raadsels uit de Noordzee. *Cranium* 24: 31-38.
- Post K, Reumer JWF. 2016. History and future of paleontological surveys in the Westerschelde Estuary (Province of Zeeland, the Netherlands). *Deinsea* 16: 1-9.
- Post K, Hoekman A, de Wilde B. 2017. Oerwalvissen op de bodem van de Noordzee. *Cranium* 34: 46-49.
- Powell, A.J., 1992. Dinoflagellate cysts of the Tertiary System. In: Powell, A.J.. A stratigraphic index of dinoflagellate cysts: 155-272.
- Ratcliffe JF. 1980. The arterial anatomy of the adult human lumbar vertebral bod: a microarteriographic study. *Journal of Anatomy* 131: 57-79.
- Schouten S. 2011. De wervels van Basilosauridae: een overzicht van en een vergelijking met raadselachtige vondsten uit de Noordzee. *Cranium* 28: 17-25.
- Steurbaat E, King C, Matthijs J, Noiret C, Yans J, Van Simaey S. 2015. The Zemst borehole, first record of the EECO in the North Sea Basin and implications for Belgian Ypresian -Lutetian stratigraphy. *Geologica Belgica* 18: 147-159.
- Stromer von Reichenbach, E. 1908. Die Archaeoceti des ägyptischen Eozäns. *Beiträge zur Paläontologie und Geologie Österreich- Ungarns und des Orients Wien* 21: 106-178.
- Uhen MD. 1999. New Species of protocetid archaeocete whale, *Eocetus wardii* (Mammalia: Cetacea) from the Middle Eocene of North Carolina. *Journal of Paleontology* 73: 512-528.
- Uhen MD. 2001. New material of *Eocetus wardii* (Mammalia, Cetacea) from the Middle Eocene of North Carolina. *Southeastern Geology* 40: 135-148.
- Uhen MD, Berndt HJ. 2008. First record of the archaeocete whale family Protocetidae from Europe. *The Fossil Record, Museum für Naturkunde, der Humboldt Universität zu Berlin* 11: 57-60.
- Van Beneden PJ. 1883. Sur quelques ossements de cétacés fossiles, réunis dans des couches phosphatées entre l'Elbe et le Weser. *Bulletin de l'Académie Royale des sciences, des lettres et des Beaux-Arts* 6: 27-33.

808

809 Vandenberghe N, Van Simaey S, Steurbaut E, Jagt JWM, Felder PJ. 2004.
810 Stratigraphic architecture of the Upper Cretaceous and Cenozoic along the southern
811 border of the North Sea Basin in Belgium. *Netherlands Journal of Geosciences/
812 Geologie en Mijnbouw* 83: 155-171.

813

814 Van Leeuwen RJ, 2000. De stratigrafie van het Oligoceen en Mioceen op het Venlo
815 Blok: kalkige microfossielen, logs en sequenties. *TNO-NITG* 00-16-B, 67 pp.

816

817 Van Vliet HJ, Bosselaers M, Vahldiek BW, Paymans Th, Verheijen I. 2020. Eocene
818 cetaceans from the Helmstedt region, Germany, with some remarks on *Platyosphys*,
819 *Basilotritus* and *Pachycetus*. *Cainozoic Research* 20: 121-148.

820

821 Van Vliet HJ, Bosselaers M, Post K. 2022. Palaeocene cetaceans (Basilosauridae) from
822 the Belgian-Dutch coastal waters. *Deinsea* 20: 1-34.

823

824 Van Vliet HJ, Bosselaers M, Paijmans Th, Calzada S. 2023. An archaeocete vertebra
825 re-examined: indications for a small-sized species of *Pachycetus* from Spain, Europe.
826 *Deinsea* 21: 1-16.

827

828 Weems, R.E., Edwards, L.E., Osborne, J.E. & Alford, A.A. 2011. An occurrence of the
829 protocetid whale "*Eocetus*" *wardii* in the Middle Eocene Piney Point Formation of
830 Virginia. *Journal of Paleontology* 85: 271-278.

831

832 Williams GL, Stover LE, Kidson EJ . 1993. *Morphology and stratigraphic ranges of
833 selected Mesozoic-Cenozoic dinoflagellate taxa in the northern hemisphere*. Geological
834 Survey of Canada, paper 92-10. 139 pp.

835

836 Zevenboom D, 1995. *Dinoflagellate cysts from the Mediterranean Late Oligocene and
837 Miocene*. Ph.D. University of Utrecht: 221 pp.

Table 1 (on next page)

Vertebral dimensions NMR-16642, *Pachycetus* sp. from Het Scheur, Belgian-Dutch border (in mm.)

TABLE 1: VERTEBRAL DIMENSIONS NMR999100016642, *PACHYCETUS* SP. FROM HET SCHEUR, BELGIAN-DUTCH BORDER (in mm)

Het Scheur	Vertebra	Length	Width NA	Width (max + pr tr)	Width	Height	Rel L = Ld/Wa	Rel W = Wa/Ha	References
NMR-16642	Th**)	111 (dors) 110 (vent)	79 (+ped) 46 (inner part)	156	101 (ant) 102 (post)	80 (ant) 83.5 (post)	1,10	1.26	This article

**), without epiphyses

Abbreviations:

ant, anterior; dors, dorsal; Ha, anterior height; L, length; Ld, dorsal length; max, maximum; NA, neural arch; post, posterior; pr tr, transverse processes; Rel, relative; Th, thoracic vertebral centrum; vent, ventral; Wa, anterior width; /, fraction

Table 2(on next page)

Vertebrae mentioned in the Figures

TABLE 2: VERTEBRAE MENTIONED IN THE FIGURES

Vertebrae mentioned in the Figures.

Collection number & taxon	Figure	Vertebra	Country & age	Length	Width	Height	Rel L= Ld/Wa	References
Type 1a: elongated vertebrae (small)								
NMR999100016642 <i>Pachycetus</i> sp., small species	4; 5A1-2; 6B-C; 7A; 8; 9; 10a1-3; 12A; 13A; 14A; 16A; 18A; 19A; 20A	Post Th**)	Het Scheur, Belgian-Dutch border; Bartonian	111 (dors) 110 (vent)	101 (ant) 102 (post)	80 (ant) 83.5 (post)	1.10	This article
NCSM 11284. <i>Pachycetus wardii</i>	7B1	Th11*)	North Carolina; Lutetian-Bartonian	? (dors) 111 (ventr)	86 (ant) 109 (post)	73 (ant) 81 (post)	1.29 (Lv)	Uhen, 2001: table 1
NCSM 11284. <i>Pachycetus wardii</i>	7B2	Th12**)	North Carolina; Lutetian-Bartonian	? (dors) 118 (ventr)	97 (ant) 112 (post)	82 (ant) 86 (post)	1.22 (Lv)	Uhen, 2001: table 1
FSAC Bouj-7 <i>Antaecetus aithai</i>	7C	Th12	Guéran, Morocco, Bartonian	128	e97 (ant) 96 (post)	e82 (ant) 77 (post)	e1.32	Gingerich & Zouhri, 2015: table 2
Type 1b: elongated vertebrae (large)								
NMR999100012331 <i>Pachycetus</i> sp., large species	7D1; 10B; 12B; 13B; 14B; 16B; 18B; 19B; 20B; 21A	Post Th**)	Het Scheur, Belgian-Dutch border; Bartonian	163 (dors) 158 (vent)	127 (ant) 147 (post)	107 (ant) 102 (post)	1.28	Van Vliet et al., 2022
NMR999100012332 <i>Pachycetus</i> sp., large species	6A, C; 7D2; 14C	Post Th**)	Het Scheur, Belgian-Dutch border; Bartonian	162 (dors) 155 (vent)	132 (ant) 152 (post)	109 (ant) 114 (post)	1.23	Van Vliet et al., 2022
NMR99910003404 <i>Pachycetus</i> sp., large species	10C; 12C; 14D	Lu	Het Scheur, Belgian-Dutch border; Bartonian	>208 (dors) >165 (vent)	>150 (ant) e175 (post)	e125 (ant) 124 (post)	?	Van Vliet et al., 2022
NsT90 <i>Pachycetus robustus</i>	5B; 7E	Posterior Th (?ant Lu) **)	Helmstedt region, Germany; Bartonian-Priabonian	166 (dors) 162 (vent)	>114 (ant) 129 (post)	>81 (ant) 96 (post)	<1.46 (>1.28) (Ld/Wp)	Van Beneden, 1883; Kuhn, 1935; Van Vliet et al., 2020: appendix table 2a
<i>Pachycetus paulsonii</i>	7F	Th	Chyhyryn, Ukraine; Bartonian-Priabonian	165	140	100	1.18	Brandt, 1873; Kellogg, 1936: table 25
KOM 44761 P 203 <i>Basilotritus uheni</i> (cf. <i>Pachycetus paulsonii</i>)	7G	ThB (12 or 13) **)	Vlavoroska, Ukraine Bartonian-Priabonian	170	110 (ant) 149 (post)	96 (ant) 108 (post)	1.55	Gol'din & Zvonok, 2013, appendix 3

ID20-4 <i>Pachycetus</i> sp.	15A	Conus, Lu	Helmstedt region, Germany; Bartonian-Priabonian	?	?	?	?	
SMNS 10934b, <i>Pachycetus</i> sp.	15B	Conus, Lu?	Mokattam, Cairo Egypt; Bartonian	?	?	?	?	Stromer, 1908; Gingerich et al., 2022
USNM 510831 <i>Basilosaurus cetoides</i>	10D; 12D	Lu/Ca	?	?	?	?	?	Houssaye et al., 2015: fig. 14
Type 2: not-elongated vertebrae								
NMR999100010284 Indeterminable basilosaurid	11A; 12E; 13C; 17A; 18C; 19C; 20C; 21B	Th/Lu**)	Wielingen/ Het Scheur, Belgian-Dutch border; Bartonian-Priabonian	177 (dors) 170 (vent)	>190 (ant) e>187 (post)	> 180 (ant) > 183 (post)	< 0.93	Van Vliet et al., 2022
Type 3: 'shortened' vertebrae								
NMR999100010283 Indeterminable basilosaurid	11B; 12F; 13D; 17B; 18D; 19D; 20D; 21C	Ca	Wielingen/ Het Scheur, Belgian-Dutch border; Bartonian-Priabonian	127 (dors) 135 (vent)	210 (ant) 212 (post)	191 (ant) 185 (post)	0.60	Van Vliet et al., 2022

5

6

7 *) , One epiphysis missing; **), both epiphyses missing

8 *Abbreviations:*

9 ant, anterior; Ca, caudal vertebral centrum; dors, dorsal; e, estimated; et al., et alii; Ld, dorsal length; Lu,
10 lumbar vertebral centrum; Lv, ventral length; post, posterior; rel, relative; Th, thoracic vertebral centrum;
11 sp, species; vent, ventral; Wa, anterior width; Wp, posterior width;?, unknown; >, more than; <, less than;
12 /, fraction

13

Table 3(on next page)

Compactness of vertebra NMR-16642 from Het Scheur, Belgian-Dutch border: anterior conus.

TABLE 3A
COMPACTNESS OF VERTEBRA NMR-16642 FROM HET SCHEUR AT THE BELGIAN-DUTCH
BORDER: ANTERIOR CONUS

Region anterior conus	Section	Compactness (Co)	Surface (Su) (in cm)	Sum value (Co.Su)	Mean value
Cortex & conus					
Midpart lateral left	1	0.897	1.5 x 1.2	1.6146	
Ventral left	2	0.828	1.5 x 1.2	1.4904	
Midline ventral	3	0.794	1.5 x 1.2	1.4292	
1-3			5.40	4.5342	0.840
Conus dorsal					
Left	4	0.774	1.5 x 1.2	1.3932	
Midline	5	0.656	1.5 x 1.2	1.1808	
4-5			3.6	2.574	0.720
conus central					
Midline left	6	0.534	1.5 x 1.2	0.9612	
Midline right	7	0.625	1.5 x 1.2	1.1250	
Left	8	0.715	1.5 x 1.2	1.2870	
6-8			5.40	3.3732	0.625
Total compactness 1-8			14.40	10.4814	0.728

Table 4(on next page)

Compactness of vertebra NMR-16642 from Het Scheur, Belgian-Dutch border: vertebral midpart

TABLE 3B
COMPACTNESS OF VERTEBRA NMR-16642 FROM HET SCHEUR AT THE BELGIAN-DUTCH
BORDER: VERTEBRAL MIDPART

Region axial midpart	Section	Compactness (Co)	Surface (Su) (in cm)	Sum value (Co.Su)	Mean value
Cortex lat					
Dorsal left	1	0.668	15 x 12	1.2024	
Dorsal right	2	0.704	12 x 15	1.2672	
1-2			3.6	2.4696	0.686
Cortex					
Pr tr right	3	0.841	12 x 15	1.5138	
3			1.8	1.5138	0.841
Cortex ventral					
Left	4	0.669	15 x 12	1.2042	
Right	5	0.680	19 x 16	2.0672	
4-5			4.84	3.2714	0.676
Central part					
Dorsal left	6	0.486	15 x 12	0.8748	
Midpart right	7	0.400	15 x 12	0.7200	
Midpart left	8	0.455	15 x 12	0.8190	
Midline left	9	0.578	15 x 12	1.0404	
central midline right	10	0.582	15 x 12	1.0476	
6-10			9.0	4.5018	0.500
Total compactness 1-10			19.24	11.7566	0.611

Table 5(on next page)

captions

Figure 1. **Location of the fossil site.** (A) Map of Belgium and the Netherlands, modified after [Van Vliet et al., 2022, fig 1](#). (B) the location of the tidal channels Wielingen and Het Scheur at the Belgian-Dutch border.

Figure 2. **Section of the Eocene strata at the fossil site.** Stratigraphy of the Paleogene and Neogene sediments in the region of Wielingen/Het Scheur at the Belgian-Dutch border: (A) Paleogene and Neogene strata directly beneath the Pleistocene and Holocene sediments at the seafloor, modified after Du Four et al., 2006, fig.3. The place where vertebra NMR-16642 has been found, is indicated with a red ellipsis. (B) The tilting of the Paleogene strata toward the north-northeast in the study area (modified after Du Four et al., 2006, fig.4). (C) Section of the Zelzate and Maldegem Formation, modified after [De Smet, et al., 1997, tabel 2.1](#), [Vandenberghie et al., 2004, fig.6](#), [Steurbaut et al., 2015, figs.3, 4](#). Corrections for the ages after [Bujak & Mudge, 1994](#); [Eldrett et al., 2004](#) and [Gradstein et al., 2020, table 28.1 & 28.2](#).

Fig. 3. Distribution chart of dinoflagellate cysts. Abbreviations: MP Miscellaneous fossils, SP Sporomorphs (bisaccate pollen and spores)

Figure 4. **Section correlated with encountered dinoflagellates.** Part of the section with age-diagnostic dinoflagellates in the sediments originally adhering to vertebra NMR-16642.

Figure 5. **Study vertebral centrum NMR-16442.** Vertebral centrum, *Pachycetus* sp., NMR-16442, from Het Scheur at the Belgian-Dutch border, in anterior (A), posterior (B), dorsal (C), ventral (D), left lateral (E) and right lateral (F) view. Arrow in 4e indicates the fovea for the rib. Scale bar is 10 cm. See also Table 1, 3.

Figure 6. **Comparison of NMR-16442 with NsT90.** (A1-2) Vertebral centrum, *Pachycetus* sp., NMR-16442, from Het Scheur at the Belgian-Dutch border. (B1-2) Vertebral centrum, *Pachycetus robustus*, NST90 (holotype) from the Helmstedt region, Germany in ventral (A1, B1) and anterior (A2, B2) view, originally described by [Van Beneden, 1883](#), modified after [Van Vliet et al., 2020](#). Scale bar is 10 cm. See also Table 3.

Figure 7. **Axial cross section NMR-16642 & NMR-12332.** Axial cross sections of the vertebral centrum NMR-16642 compared with that of the vertebral centrum NMR-12332, both from Het Scheur at the Belgian-Dutch border, showing that NMR-16642 completely falls within the inner boundaries of the multi-layered cortex of NMR-12332. This indicates that NMR-16642 is from a different, smaller species of *Pachycetus* than the large *Pachycetus* sp., NMR-12332. (A) Axial cross section of NMR-12332. (B) Axial cross section of NMR-16642 (A-B axial sections through the vertebra's midpart). (C) Projection of NMR-16642 upon NMR-12332 (axial section through the anterior conus). Red arrows indicate the external and internal boundaries of the multi-layered cortex of NMR-16642; blue arrows indicate the external and internal boundaries of the multi-layered cortex of NMR-12332. See also Table 3. Scale bar is 50 mm.

Figure 8. **Plot of vertebrae assigned to the genus *Pachycetus*.** Scatter diagram with width plotted against length of posterior thoracic vertebral centra, all assigned to *Pachycetus* spp., showing two different clusters of vertebrae. The spheres 'A'-'C' within the ellipsis to the left, represent vertebrae belonging to small-sized species, plus vertebra NMR-16642. Vertebra NMR-16642 from Het Scheur at the Belgian-Dutch border is indicated by 'A'. The spheres 'D'-'G' within the ellipsis to the right, represent vertebrae, belonging to large species from Europe. 'B1-2': *Pachycetus wardii*, NCSM 11284 from North Carolina; 'C': *Antaeocetus aithai*, FSAC Bouj-7 from Guéran, Morocco; 'D1-2': *Pachycetus* sp., NMR-12331 resp. NMR-12332 from Het Scheur at the Belgian-Dutch border; 'E': *P. robustus*, NsT90, from the Helmstedt Region, Germany, Belgium; 'F': *P. paulsonii*; from Chyhyryn, Ukraine; 'G' *Basilotritus uheni* (cf. *P. paulsonii*), KOM 44761 P 203 from Vlavovska, Ukraine. See also Table 2.

Figure 9. **Different types of bone in NMR-16642.** (A1-C2) CT scan images of the posterior thoracic vertebral centrum, *Pachycetus* sp., NMR-16442 from Het Scheur, at the Belgian-Dutch border, in axial (A1-2), coronal - upper part of the centrum (B1-2), and sagittal (C1-2) sections. (A2), (B2), (C2) have been artificially embrightened in colour, to indicate different parts of the spongy bone. Dark-brown

parts show the multi-layered bone beneath the cortex (indicated by '1'), medium-beige parts show the more or less disorganised spongy bone underneath the multi-layered bone (indicated by '2'); light-yellowish parts show the conus (indicated by '3'). See also Table 3. Scale bar is 100 mm.

Fig. 10. Compactness measurements. Sections of the vertebral centrum, *Pachycetus* sp., NMR-16442 from Het Scheur at the Belgian-Dutch border, in axial view, used for measuring the bone compactness: (A) Anterior conus. (B) Vertebral midpart. See also table 3. Scale bar in (A) and (B) is 50 mm. Scale bars left and right below is 15 mm.

Fig. 11. Structure of the cortex, Morphotype 1a, b. CT-scan images from the midpart of vertebral centra of several basilosaurid taxa, Morphotype 1a, small species of *Pachycetus*, Morphotype 1b, large species of *Pachycetus* and *Basilosaurus cetoides* (elongated vertebrae) in axial view. (A) Vertebral centrum, *Pachycetus* sp., NMR-16642 from Het Scheur at the Belgian-Dutch border in total view (A1), part of the lateral cortex (A2), part of the ventral cortex (A3). (B) Vertebral centrum, *Pachycetus* sp., NMR-12331 from Het Scheur at the Belgian-Dutch border in total view (B1), part of the lateral cortex (B2), part of the ventral cortex (B3). (C) Vertebral centrum, *Pachycetus* sp., NMR-3404 from Het Scheur at the Belgian-Dutch border, in axial view. (D) Lumbar or caudal vertebral centrum, *Basilosaurus cetoides*, USNM 510831, in axial view, modified after Houssaye et al., 2015: fig. 14a. Vertical arrow downward in (A1), (B1), (C) and (D) points to the ventral cortex; vertical arrow upward points to the thin dorsal cortex. 1a-b, 2 in (D): 1a, compact outer layers of the cortex; 1b in (D): spongy-like inner layers of the cortex; 2 in (D): spongy bone at the midpart of the vertebral; centrum; compare with Fig. 8b. See also Table 3. Scale bars are 50 mm.

Fig. 12. Structure of the cortex, Morphotype 2-3. CT-scan images from the midpart of vertebral centra of two basilosaurid taxa, Morphotype 2 (not-elongated vertebrae) and Morphotype 3 ('shortened' vertebrae, both from Wielingen/Het Scheur at the Belgian-Dutch border, in axial view. (A) Vertebral centrum, indeterminate basilosaurid species, NMR-10284, in total view (A1), and a part of the ventral cortex (A2). Horizontal red arrows point to layers with a loose structure, intercalated between compact layers. (B) Vertebral centrum, NMR-10283, indeterminate basilosaurid, Morphotype 3, in total view (B1), part of the left lateral cortex (B2) and part of the left ventral cortex (B3). Vertical arrows in (A1) and (B1) downward points to the ventral cortex; vertical arrow upward in (A1) and (B1) points to the thick dorsal cortex, contrary to what is seen in vertebrae of Morphotype 1. Horizontal arrows in (A2) point to less compact layers, intercalated between compact layers in the cortex. See also Table 3. Scale bars are 50 mm.

Fig. 13. Comparison of basilosaurid vertebrae in sagittal section. Sections at the midpart of vertebral centra of several basilosaurid taxa, vertebral centra, Morphotype 1a, 1b, 2, 3 from Wielingen/Het Scheur at the Belgian-Dutch border (except (D), in sagittal view, showing the comparable inner structures of these centra. Morphotype 1 (elongated vertebral centra): (A-D); Morphotype 2 (not-elongated vertebral centra): (E); Morphotype 3 ('shortened' vertebral centra): (F). (A) Vertebral centrum, *Pachycetus* sp., NMR-16642, Morphotype 1a. (B) Vertebral centrum, *Pachycetus* sp. NMR-12331 Morphotype 1b. (C) Vertebral centrum, *Pachycetus* sp., NMR-3404 Morphotype 1b. (D) Vertebral centrum, *Basilosaurus cetoides*, USNM 510831, modified after Houssaye et al., 2015: fig. 14b. (E) Vertebral centrum, indeterminate basilosaurid species, NMR-10284 Morphotype 2. (F) Vertebral centrum, indeterminate basilosaurid, NMR-10283 Morphotype 3. The shape of the posterior conus is indicated by a white line. See also Table 3. Scale bars are 50 mm.

Fig. 14. Structure of the conus. CT-scan images of a part of the posterior conus of several basilosaurid vertebral centra, Morphotype 1a, 1b, 2, 3 from Wielingen/Het Scheur at the Belgian-Dutch border. (A) Thoracic centrum, *Pachycetus* sp., NMR-16642, Morphotype 1a, in sagittal (A1) and coronal (A2) view. (B) Thoracic vertebral centrum, *Pachycetus* sp., NMR-12331, Morphotype 1b, in sagittal (B1) and coronal (B2) view. (C) Thoracic or lumbar vertebral centrum, indeterminate basilosaurid species, NMR-10284, Morphotype 2, in sagittal view. (D) Caudal vertebral centrum, indeterminate basilosaurid, NMR-10283, Morphotype 3, in sagittal view. Red arrows in (A1-2), (B1-2) indicate the layering, seen in the conus, indicative of slower and more rapid growth. In (A1), (B1), (C) and (D) left side is posterior; in (A2) and (B2) left side is left. See also Table 3. Scale bars are 50 mm.

Fig. 15. **Vertebral vascular canals (VC)**. Comparison of the schematically figured midvertebral, epiconal and endoconal VC within vertebral centra, Morphotype 1a, small species of *Pachycetus* and 1b, large species of *Pachycetus* both from Het Scheur at the Belgian-Dutch border. All are in in right lateral (.1), left lateral (.2), posterior (.3) and anterior (.4) view. (A) Posterior thoracic vertebral centrum, *Pachycetus* sp., NMR-16642. (B) Posterior thoracic vertebral centrum, *Pachycetus* sp., NMR-12331. (C) Posterior thoracic vertebral centrum, *Pachycetus* sp., NMR-12332. (D) Lumbar vertebral centrum, *Pachycetus* sp., NMR-3404. Regarding the midvertebral VC: in NMR-16642, ventral VC are lacking, contrary to NMR-12331, NMR-12332 and NMR-3404. Multiple, rather small dorsal and ventral midvertebral VC are seen in NMR-12331 and NMR-12332. Only a few, but large midvertebral VC, ending in large fossae are seen in the lumbar NMR-3404. See also Table 3. Scale bar is 50 mm.

Fig. 16. **Epiconal vascular canals (epiconal VC), surrounding vertebra's conus**. Two conus from vertebrae of *Pachycetus*, seen from the midpart of the vertebral centrum (A) Partial anterior conus, ID20-4, of *Pachycetus* sp. from Helmstedt, Germany. (B) Conus of *Pachycetus* sp. SMNS 10934b (Stuttgart), from Mokattam, Cairo, Egypt (only the conus of the vertebra is illustrated). Red arrows indicate the epiconal VC. Only the VC that are visible at the pictures, are indicated. See also Table 3. Scale bar is 50 mm.

Fig. 17. **Epiconal vascular canals (epiconal VC)**. CT-scan images of a small and a large species of *Pachycetus* from Het Scheur at the Belgian-Dutch border. (A) Vertebral centrum, *Pachycetus* sp., NMR-16642, Morphotype 1a, in axial (A1), sagittal (A2) and coronal view (A3). (B) Vertebral centrum, *Pachycetus* sp., NMR-12331, Morphotype 1b, in axial (B1), sagittal (B2) and coronal view (B3, B4). The epiconal VC are coloured red, except in (B4). In (B4) the confluence of epiconal canals in the central vascular node is seen. Red arrows in (A2), (B2) and (B4) point to an endoconal VC. See also Table 3. Scale bar in (A1-3) and (B1-3) is 50 mm. Scale in (B4) is 10 mm.

Fig. 18. **Epiconal vascular canals (epiconal VC)**. CT-scan images of a not-elongated vertebral centrum, Morphotype 2 (A) and a 'shortened' vertebral centrum, Morphotype 3 (B), both from Wielingen/Het Scheur at the Belgian-Dutch border, in axial view, near the vertebra's midpart. (A) Vertebral centrum, indeterminable basilosaurid, NMR-10284. (B) Vertebral centrum, indeterminable basilosaurid, NMR-10283, in axial view. The epiconal VC are coloured red. See also Table 3. Scale bar is 50 mm.

Fig. 19. **Endoconal vascular canals (endoconal VC)**. CT-scan images of the anterior conus of several basilosaurid vertebral centra, morphotypes 1a, 1b, 2 and 3 from Wielingen/Het Scheur at the Belgian-Dutch border. (A) Vertebral centrum, *Pachycetus* sp., NMR-16642, Morphotype 1a, in sagittal view. The majority of the endoconal VC are hardly visible, but the branching of a large endoconal VC from an epiconal one is seen on the left. (B) Vertebral centrum, *Pachycetus* sp., NMR-12331 Morphotype 1b in sagittal view. (C) Vertebral centrum, indeterminable basilosaurid, NMR-10284, Morphotype 2, in sagittal view. The endoconal VC end between the epiphyseal ridges. The dark lining of the ridges at the epiphyseal side is interpreted as capillaries, or maybe the former places of cartilage. (D) Caudal vertebra, indeterminable basilosaurid, NMR-10283, Morphotype 3, in sagittal view. Also here, the endoconal VC end between the epiphyseal ridges. Horizontal red arrow in (A) indicates the branching of an endoconal VC from an epiconal one. Red arrows in (A), (B), (C) and (D) indicate the endoconal VC, ending between the ridges of the epiphyseal side. Horizontal red arrow in (C) indicates capillaries or maybe places where cartilage had been. See also Table 3. Scale bars are 50 mm.

Fig. 20. **Endocortical vascular canals (endocortical VC)**. CT-scan images of several basilosaurid vertebral centra, morphotypes 1a, 1b, 2 and 3 from Wielingen/Het Scheur at the Belgian-Dutch border, in coronal view through the cortex at the vertebra's ventral midline, showing the layers with endocortical VC, present in vertebrae with a loose or a compact cortex. (A) Small species of *Pachycetus* sp., NMR-16642, Morphotype 1a. (B) Large species of *Pachycetus* sp., NMR-12331, Morphotype 1b. (C1-3) Indeterminable basilosaurid, NMR-10284, Morphotype 2 showing the succession of several layers with endocortical VC. In (C1) the inner layers of the ventral cortex, (C2) more ventrally and (C3) at the ventral surface. (D) Indeterminable basilosaurid, NMR-10283, Morphotype 3 (with a very large and a smaller ventral

foramen). Red arrows in (A), (B) (C) & (D) show the anterior-posterior running endocortical VC in layers of the inner cortex. See also Table 3. Scale bars are 50 mm.

Fig. 21. **Endocortical vascular canals (endocortical VC).** CT-scan images of several basilosaurid vertebral centra, morphotypes 1a, 1b, 2 and 3 from Wielingen/Het Scheur at the Belgian-Dutch border. (A) *Pachycetus* sp., NMR-16642, cortex of the right transverse process in sagittal view. (B) *Pachycetus* sp., NMR-12331, cortex of the right transverse process in coronal section. (C) Indeterminable basilosaurid, NMR-10284, cortex near the right transverse process in coronal section. (D) Indeterminable basilosaurid, NMR-10283, cortex near the right transverse process in coronal section. Red arrows indicate the directions of the endocortical VC in layers of the inner cortex, running toward the end of the transverse process. In (A), left side is dorsal; in (B), (C) and (D), left side is left. See also Table 3. Scale bars are 50 mm.

Fig. 22. **Accessory vascular canals (accessory VC).** CT-scan images of several basilosaurid vertebral centra, morphotypes 1b, 2 and 3 from Wielingen/Het Scheur at the Belgian-Dutch border, in axial section, showing the accessory VC. (A) Large species of *Pachycetus* sp., NMR-12331, Morphotype 1b. (B) Indeterminable basilosaurid, Morphotype 2. (C) Indeterminable basilosaurid, NMR-10283, Morphotype 3. Red arrows in (A), (B) & (C) indicate the tiny accessory VC. See also Table 3. Scale bar is 50 mm.

Fig. 23. **Vascularisation in human vertebrae.** (A) Lumbar vertebrae in right lateral view, with extraosseous, perivertebral arteries, arising from the aorta and giving rise to arteries for the blood supply of the vertebral centrum. (B) Perivertebral and intraosseous arteries of the vertebral centrum in superior view. (C) Intraosseous arterial system, in coronal (C1) view, in axial view sectioned through a metaphyseal plane (C2), in sagittal (C3) view and in axial (C4) view sectioned through the equatorial plane. (D) Lumbar vertebrae in sagittal view, extra- and intraosseous veins and venous plexuses. (E) Perivertebral venous plexuses and intraosseous veins of the vertebral centrum in superior view. Note that B is schematically figured in C2. AEP, anterior external vertebral venous plexus; AIP, anterior internal vertebral venous plexus; anterolat equatorial art, anterolateral equatorial arteries; art, artery/arteries; AVB, anterior vertebral canal branch; metaphyseal anast art, metaphyseal anastomosing artery; PIP, posterior internal vertebral venous plexus. (A) Modified after Jayaraman, 2008, fig. 14-2a; fig. 4.20; (B) Modified after Moore et al., 2014, fig. 4.25; (C1-4) Modified after Ratcliffe, 1980: fig. 16. (D-E) Modified after Moore et al., 2014, fig. 4.26.

TABLES

Table 1. Vertebral dimensions NMR999100016642, *Pachycetus* sp. from Het Scheur, Belgian-Dutch border (in mm).

Table 2. Vertebrae mentioned in the Figures.

Table 3a. compactness of vertebra NMR-16642 from Het Scheur at the Belgian-Dutch border: anterior conus.

Table 3b. compactness of vertebra NMR-16642 from Het Scheur at the Belgian-Dutch border: vertebral midpart.

Figure 1

Location of the fossil site

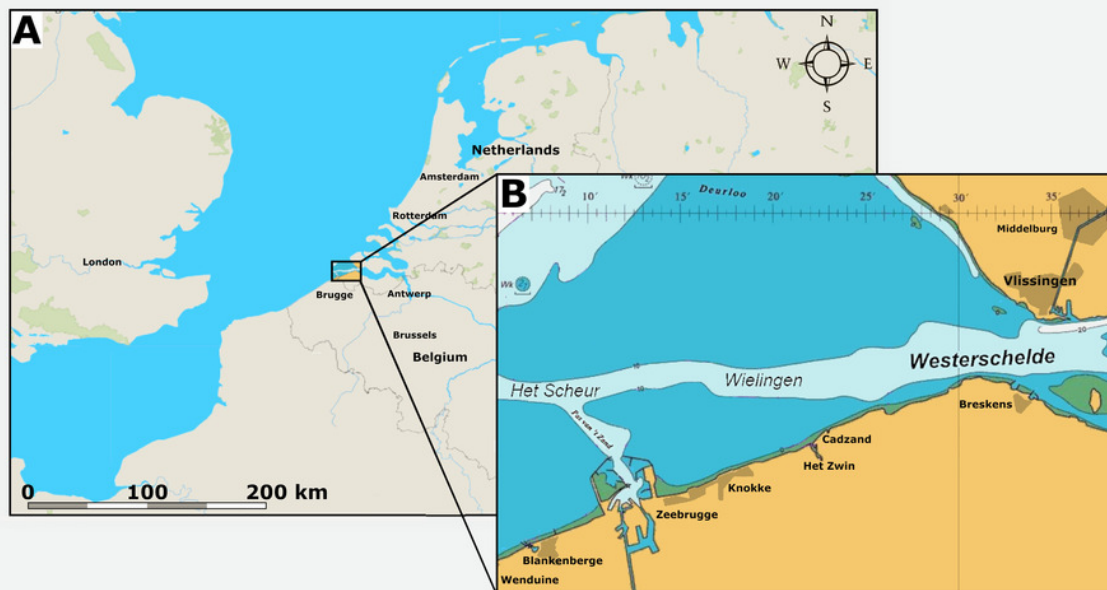


Figure 2

Section of the Eocene strata at the fossil site.

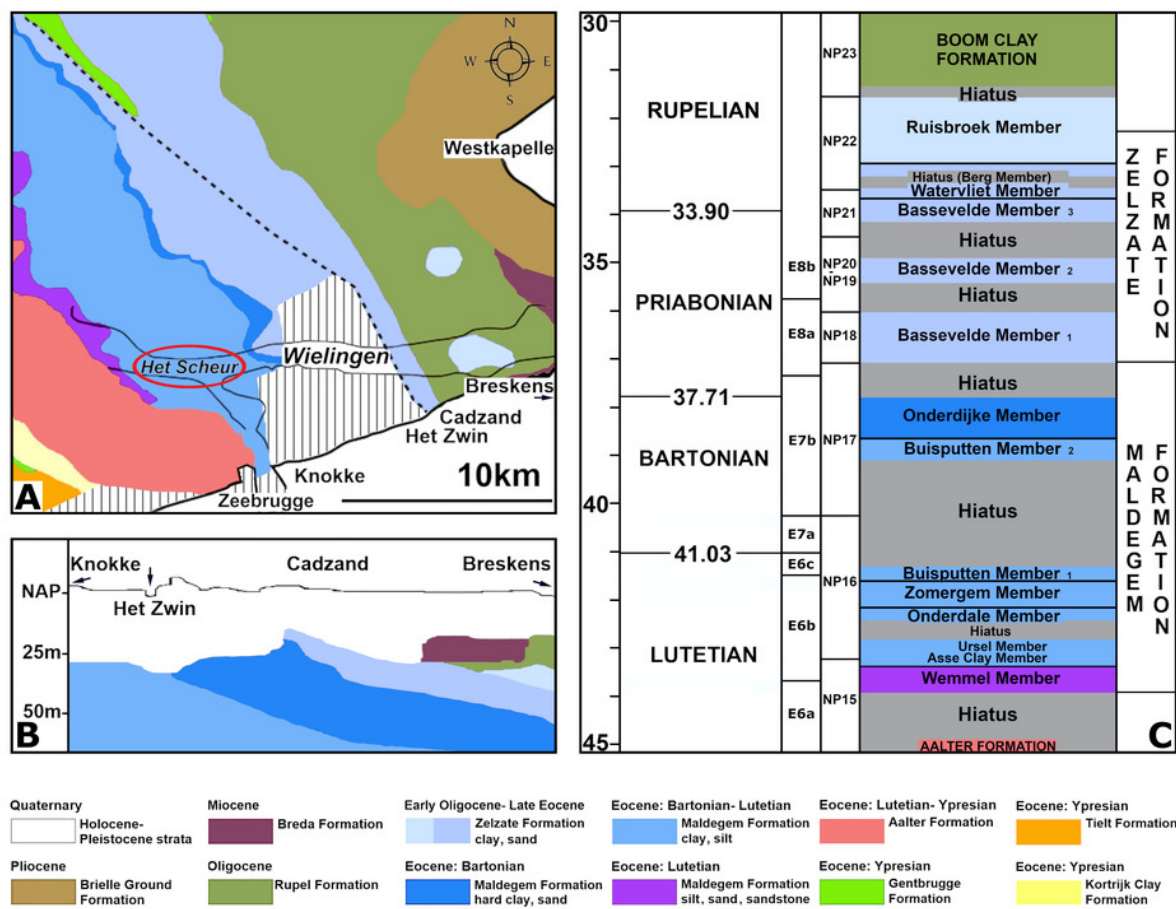


Figure 3

Distribution chart of dinoflagellate cysts.

Chronostratigraphy	Age	Bartonian, Zone E7b (Bujak & Mudge, 1994)	Dinoflagellate Cysts	
			Absolute abundance	SP
1	Adnatosphaeridium multispinosum	1	Adnatosphaeridium multispinosum	1
2	Areosphaeridium diktyoplokum	2	Areosphaeridium diktyoplokum	2
3	Areosphaeridium ebdonii	3	Areosphaeridium ebdonii	3
4	Areosphaeridium fenestratum	4	Areosphaeridium fenestratum	4
5	Areosphaeridium michoudii	5	Areosphaeridium michoudii	5
6	Cerebrocysta bartonensis	6	Cerebrocysta bartonensis	6
7	Cerodinium spp.	7	Cerodinium spp.	7
8	Charlesdowniea spp.	8	Charlesdowniea spp.	8
9	Cordosphaeridium cantharellum	9	Cordosphaeridium cantharellum	9
10	Cordosphaeridium funiculatum	10	Cordosphaeridium funiculatum	10
11	Cordosphaeridium minimum	11	Cordosphaeridium minimum	11
12	Cordosphaeridium spp.	12	Cordosphaeridium spp.	12
13	Cyclonephelium vicinum	13	Cyclonephelium vicinum	13
14	Dapsilidinium spp.	14	Dapsilidinium spp.	14
15	Deflandrea heterophlycta	15	Deflandrea heterophlycta	15
16	Deflandrea phosphoritica	16	Deflandrea phosphoritica	16
17	Dinopterygium spp.	17	Dinopterygium spp.	17
18	Diphyes pseudoficusoides	18	Diphyes pseudoficusoides	18
19	Distatodinium craterum	19	Distatodinium craterum	19
20	Distatodinium spp.	20	Distatodinium spp.	20
21	Enneadocysta pectiniformis	21	Enneadocysta pectiniformis	21
22	Fibrocysta spp.	22	Fibrocysta spp.	22
23	Genus A/B species A/B	23	Genus A/B species A/B	23
24	Glaphyrocysta spp.	24	Glaphyrocysta spp.	24
25	Heteraulacacysta spp.	25	Heteraulacacysta spp.	25
26	Homotryblum floripes/plectilum	26	Homotryblum floripes/plectilum	26
27	Homotryblum tenuispinosum	27	Homotryblum tenuispinosum	27
28	Hystrichokolpoma rigaudiae	28	Hystrichokolpoma rigaudiae	28
29	Hystrichokolpoma spp.	29	Hystrichokolpoma spp.	29
30	Lejeunecysta spp.	30	Lejeunecysta spp.	30
31	Lingulodinium machaerophorum	31	Lingulodinium machaerophorum	31
32	Melitasphaeridium asterium	32	Melitasphaeridium asterium	32
33	Melitasphaeridium choanophorum	33	Melitasphaeridium choanophorum	33
34	Melitasphaeridium pseudorecurvatum	34	Melitasphaeridium pseudorecurvatum	34
35	Operculodinium centrocarpum	35	Operculodinium centrocarpum	35
36	Operculodinium spp.	36	Operculodinium spp.	36
37	Palaeocystodinium golzowense	37	Palaeocystodinium golzowense	37
38	Pentadinium imaginatium	38	Pentadinium imaginatium	38
39	Phthanoperidinium echinatum	39	Phthanoperidinium echinatum	39
40	Phthanoperidinium spp.	40	Phthanoperidinium spp.	40
41	Rhombodinium draco	41	Rhombodinium draco	41
42	Rhombodinium rhomboideum	42	Rhombodinium rhomboideum	42
43	Rottnestia borussica	43	Rottnestia borussica	43
44	Samlandia chlamydophora	44	Samlandia chlamydophora	44
45	Selenopemphix brevispinosa	45	Selenopemphix brevispinosa	45
46	Selenopemphix nephroides	46	Selenopemphix nephroides	46
47	Spiniferites spp.	47	Spiniferites spp.	47
48	Tectodinium pellitum	48	Tectodinium pellitum	48
49	Thalassiphora fenestrata	49	Thalassiphora fenestrata	49
50	Thalassiphora pelagica	50	Thalassiphora pelagica	50
51	Wetzeliiella articulata	51	Wetzeliiella articulata	51
52	Wetzeliiella spp.	52	Wetzeliiella spp.	52
1	Bisaccates	1	Bisaccates	1
2	Osmundacidites spp.	2	Osmundacidites spp.	2
3	Reworking sporomorphs	3	Reworking sporomorphs	3
4	Varia	4	Varia	4
1	Foraminifera	1	Foraminifera	1
2	Pterospermella	2	Pterospermella	2
3	Tasmanaceae	3	Tasmanaceae	3

Figure 4

Section correlated with encountered dinoflagellates

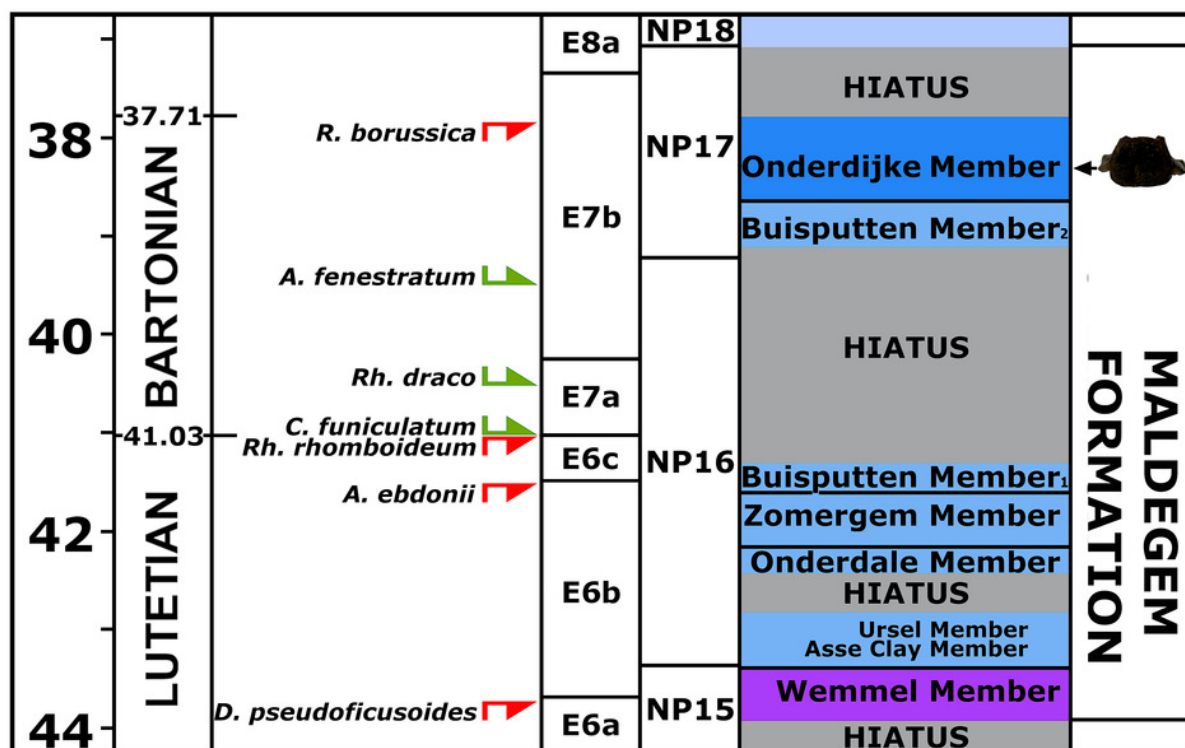


Figure 5

Study vertebral centrum NMR-16442.



A



B



C



D



E



F



Figure 6

Comparison of NMR-16442 with NsT90.

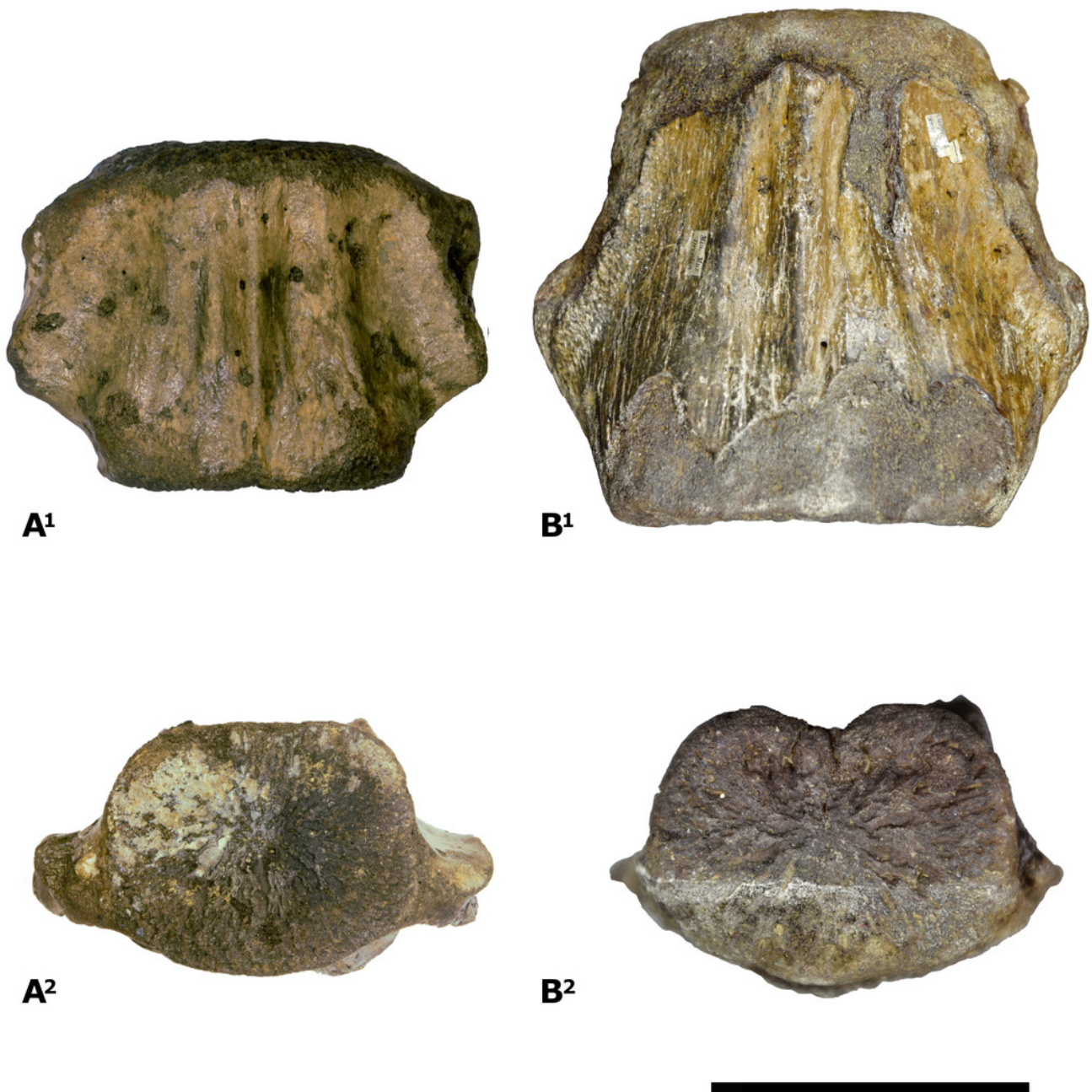


Figure 7

Axial cross section NMR-16642 & NMR-12332.

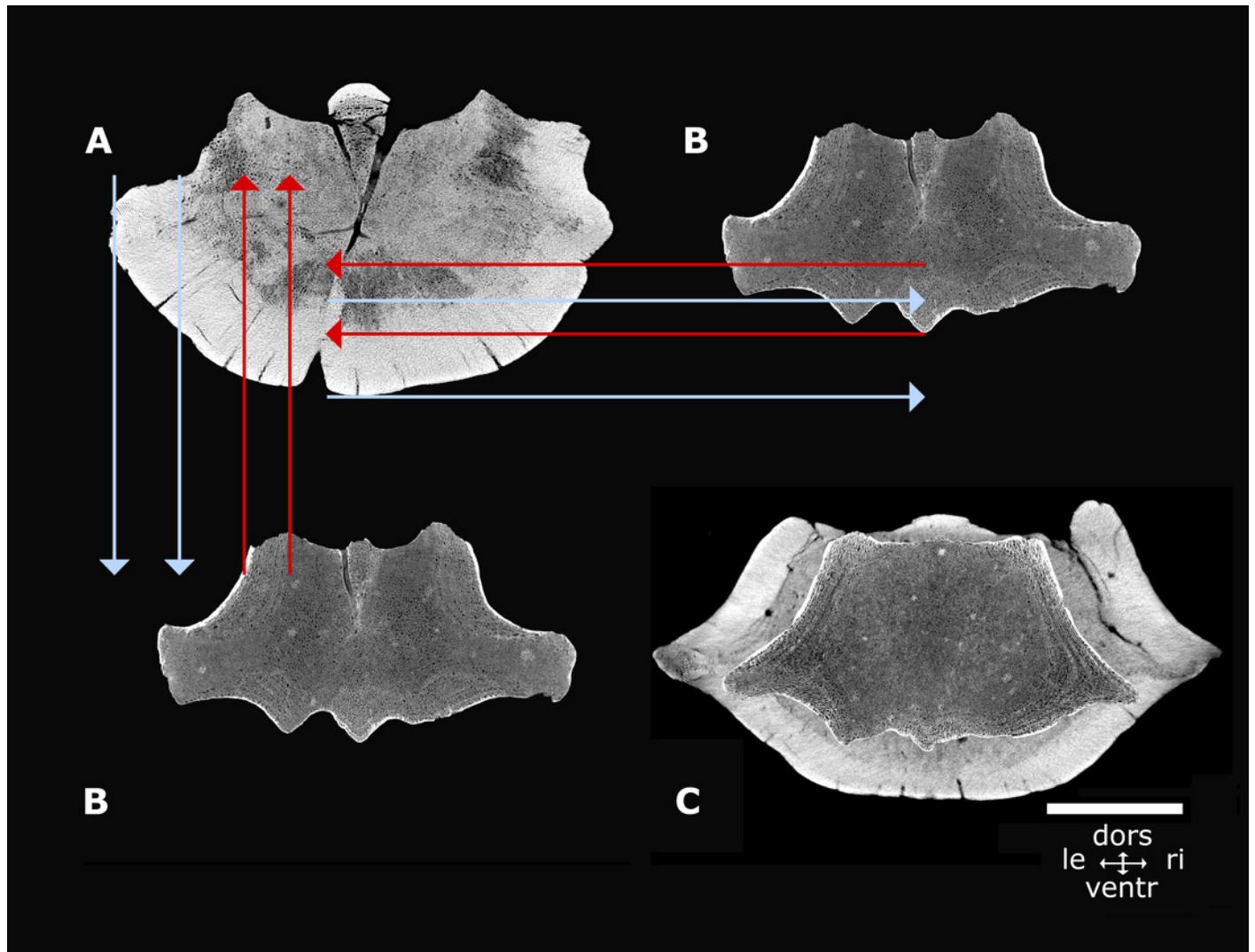


Figure 8

Plot of vertebrae assigned to the genus *Pachycetus*.

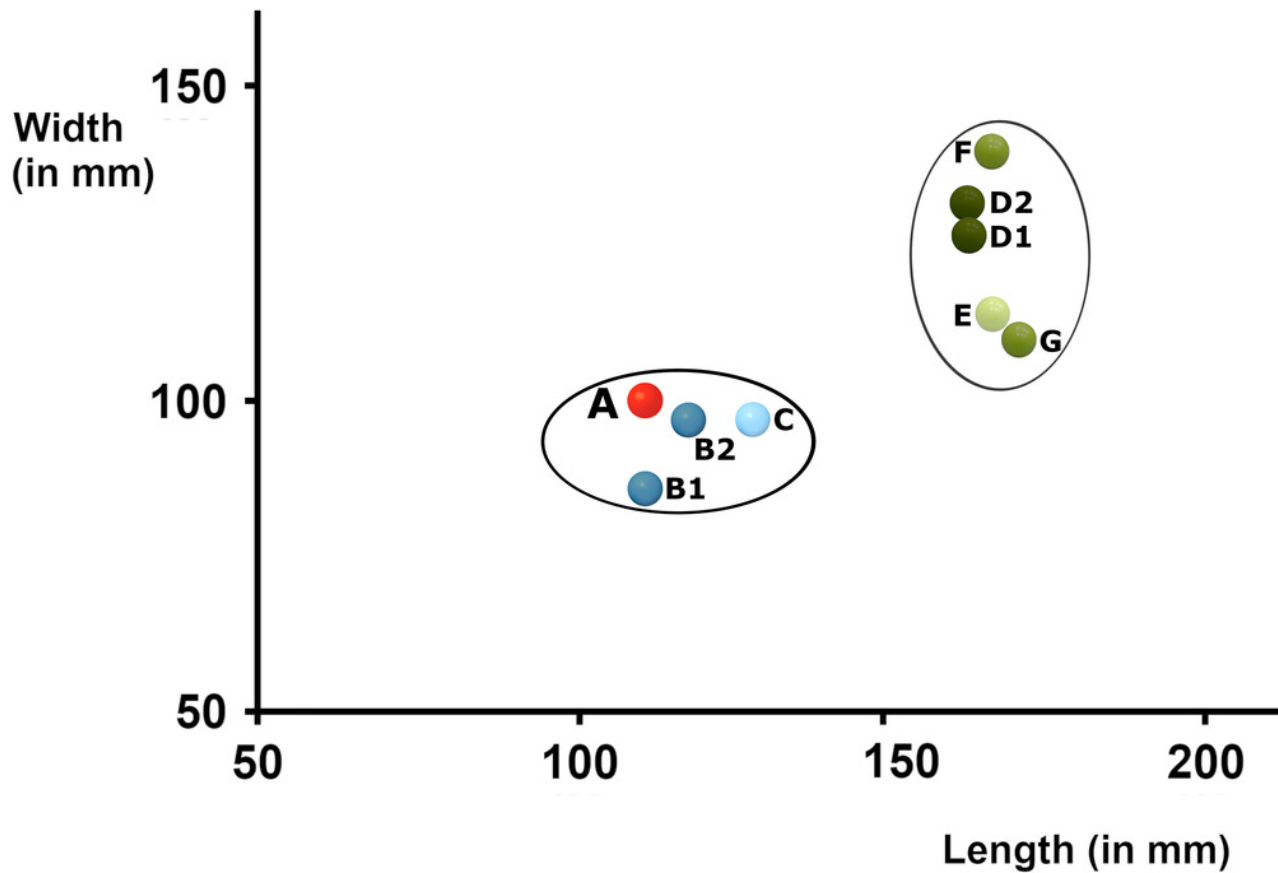


Figure 9

Different types of bone in NMR-16642.

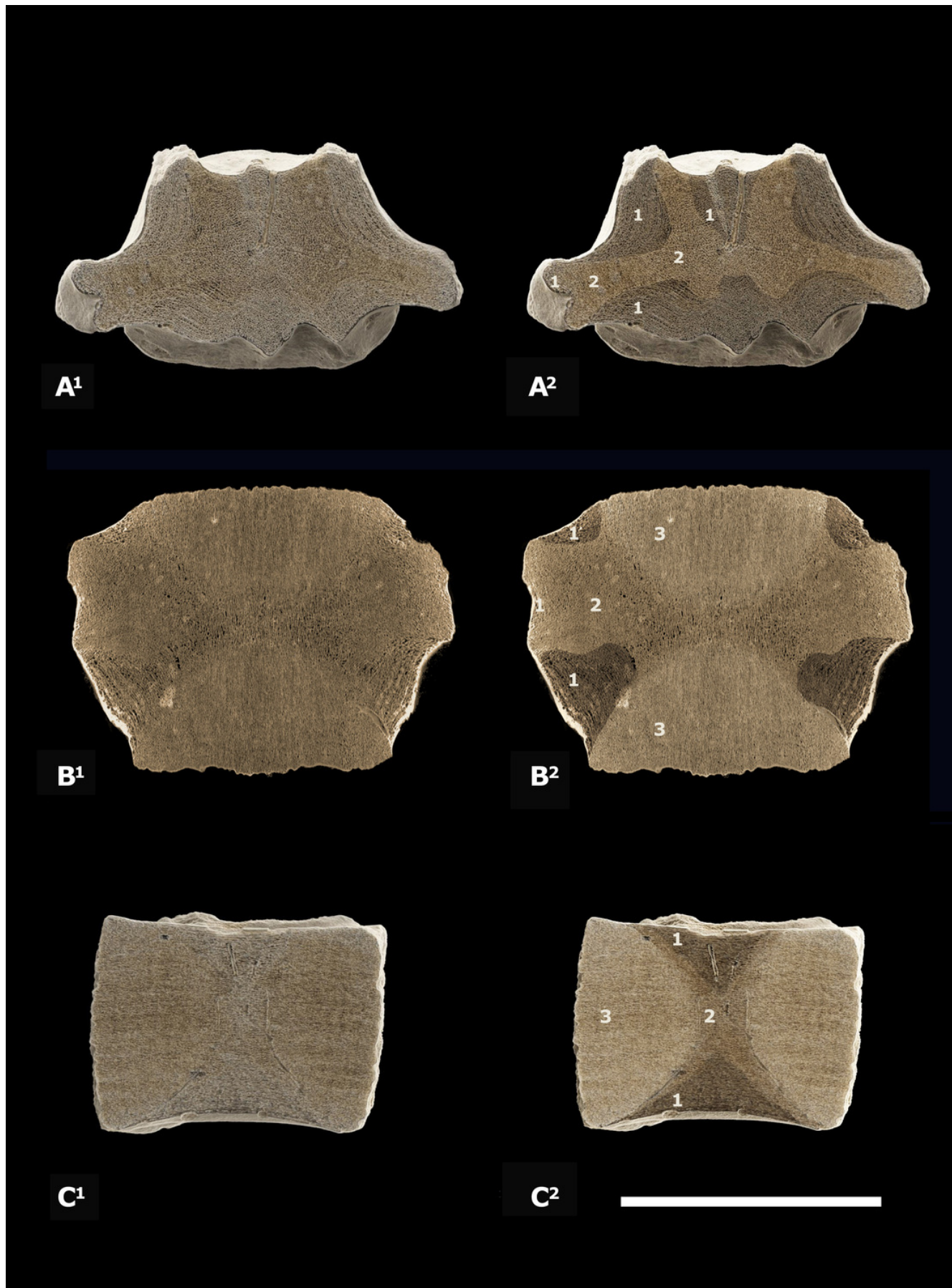


Figure 10

Compactness measurements.

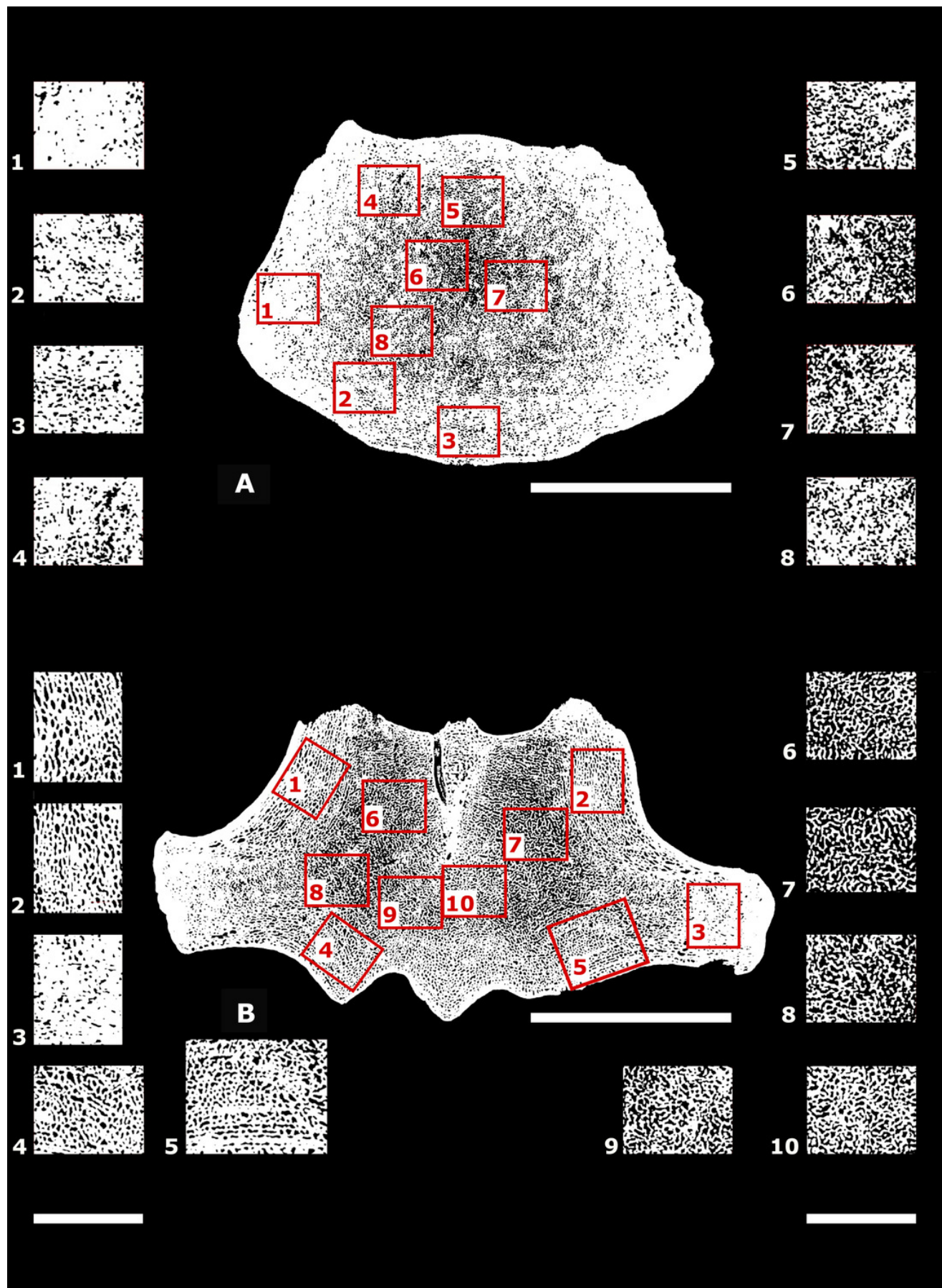


Figure 11

Structure of the cortex, Morphotype 1a, b.

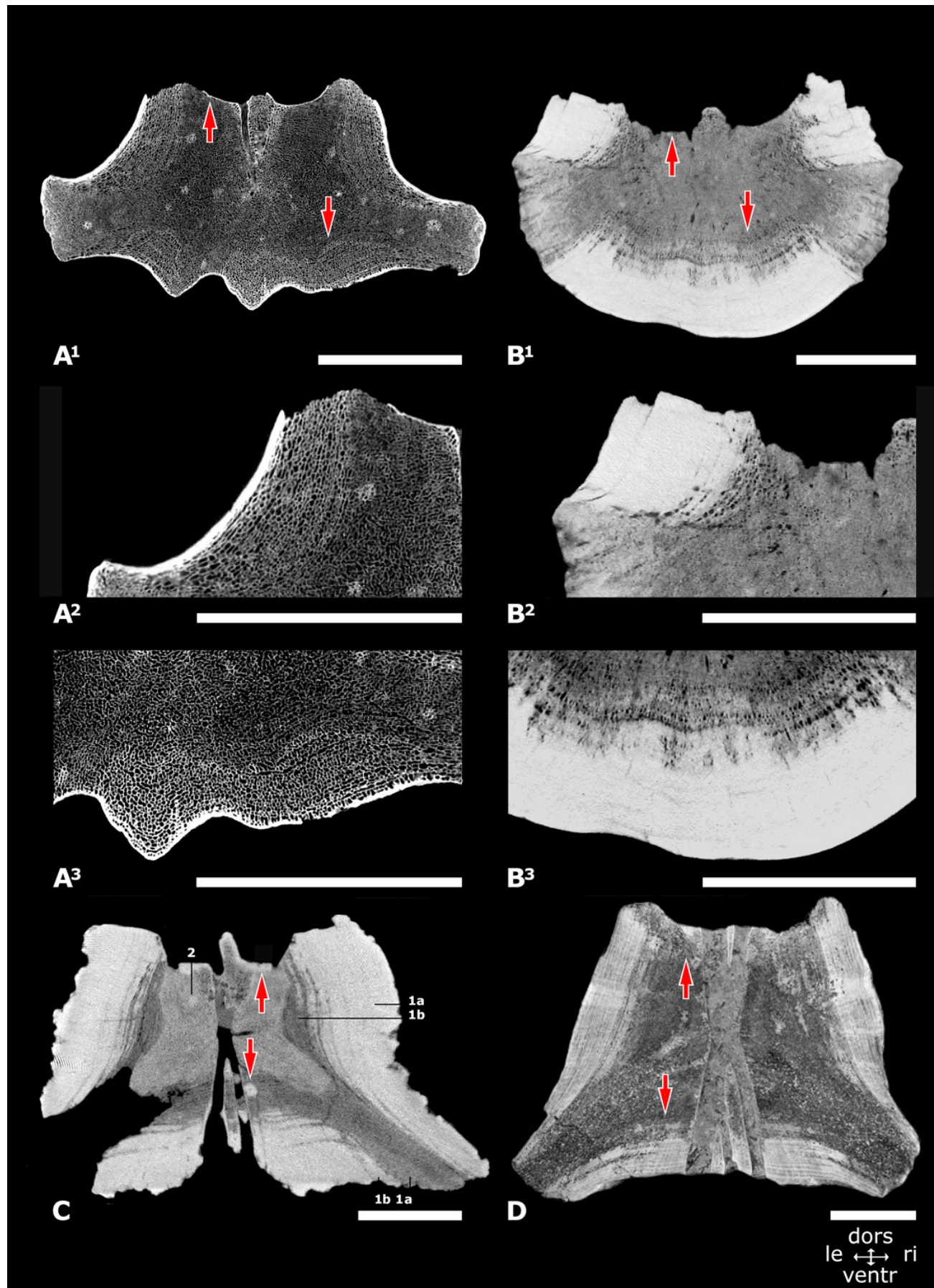


Figure 12

Structure of the cortex, Morphotype 2-3.

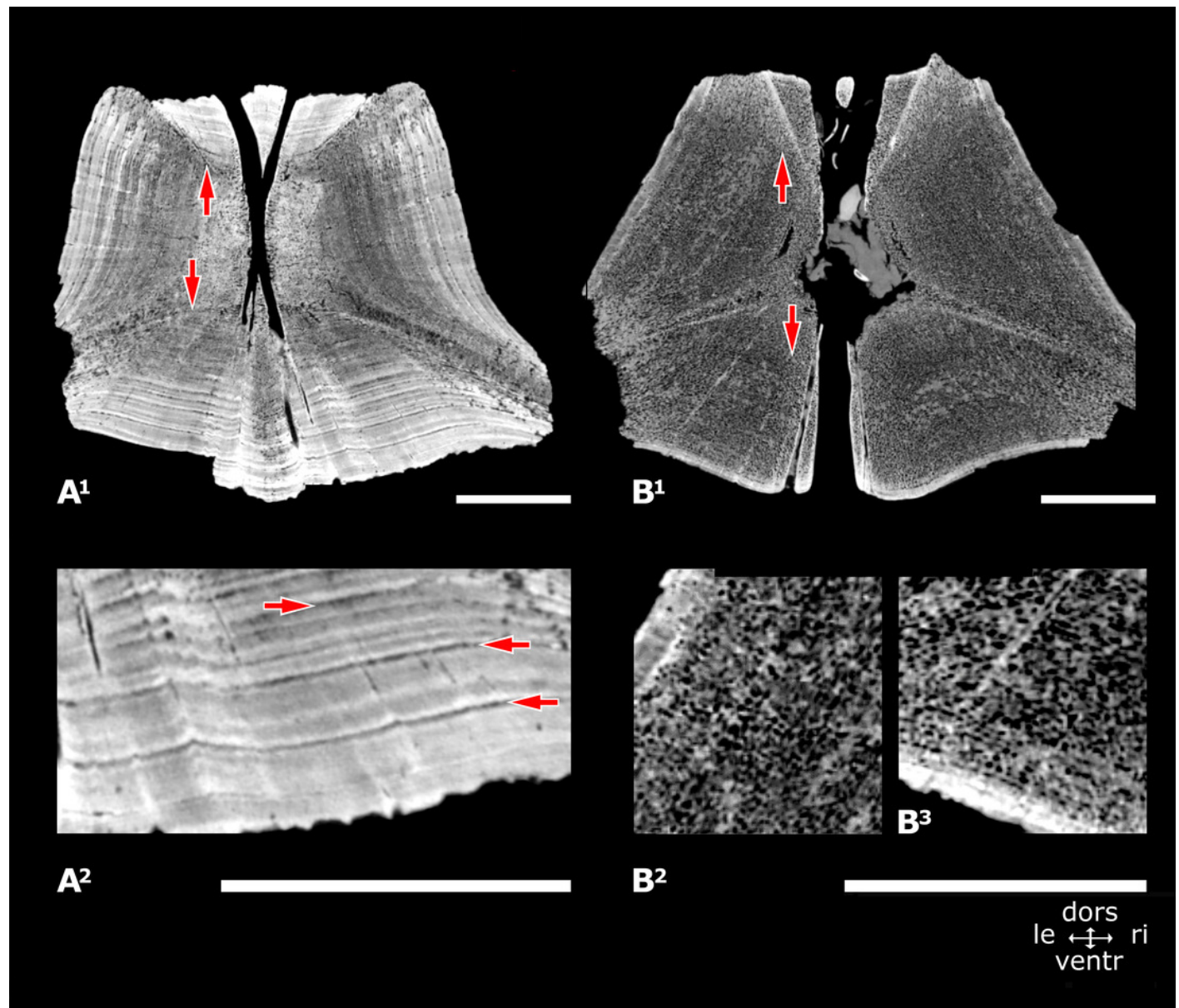


Figure 13

Comparison of basilosaurid vertebrae in sagittal section.

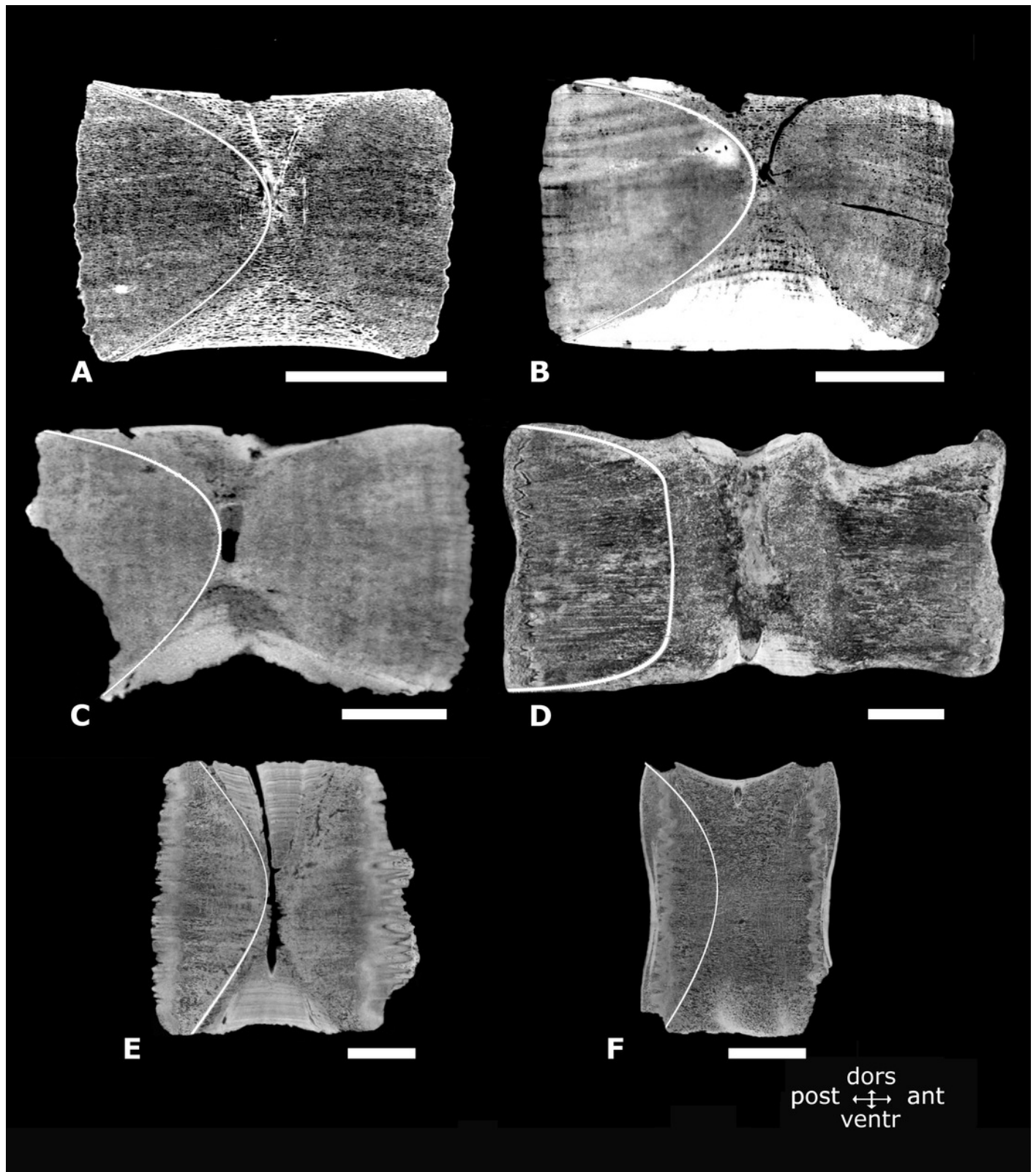


Figure 14

Structure of the coni.

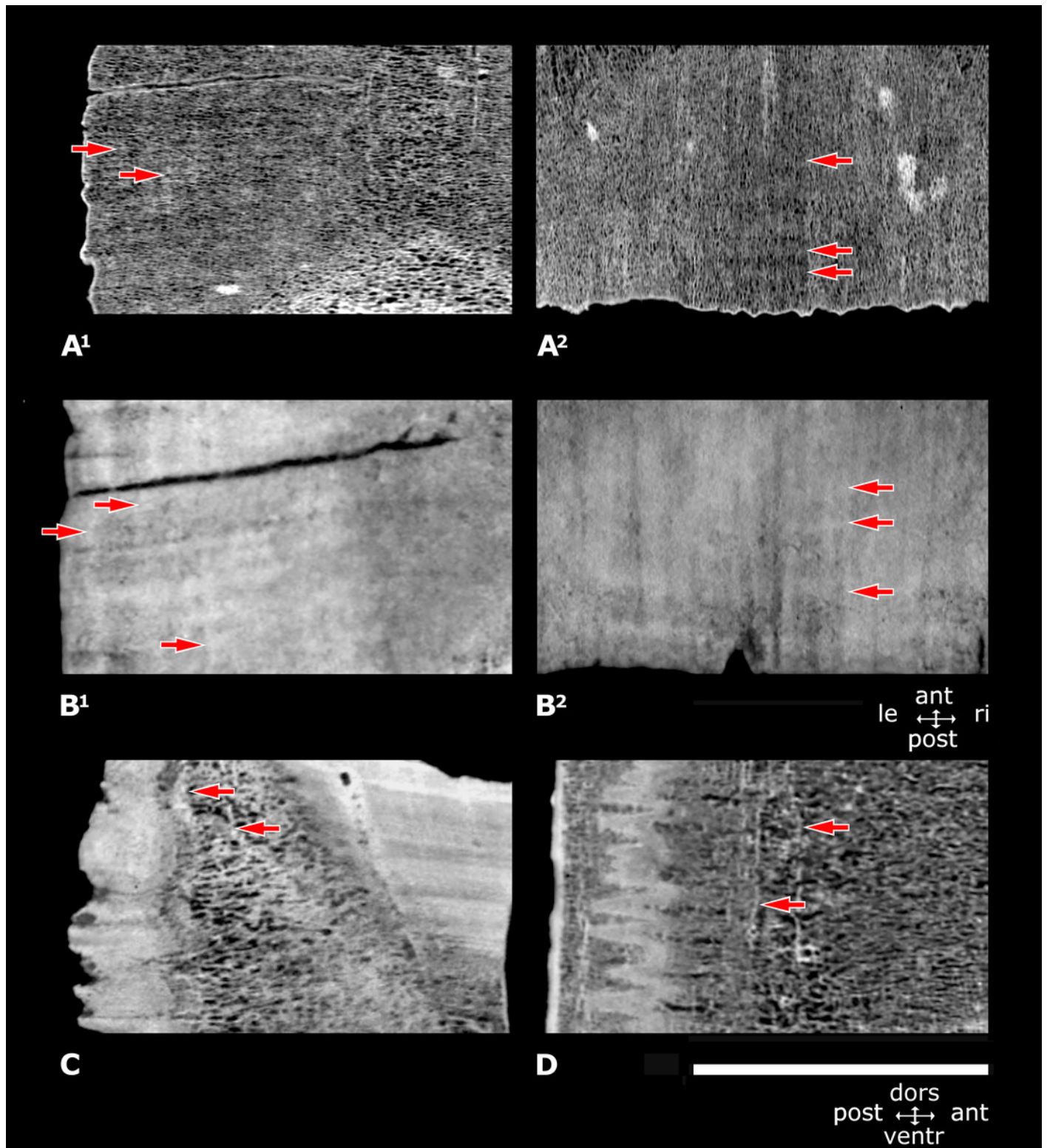


Figure 15

Vertebral vascular canals (VC).

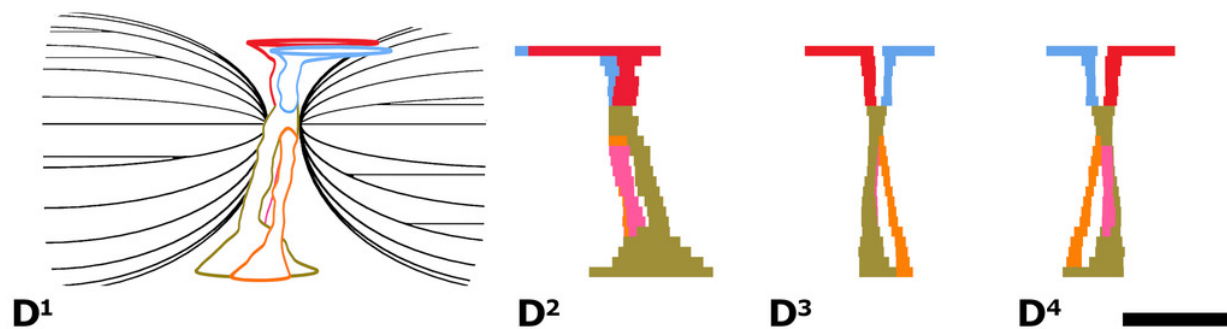
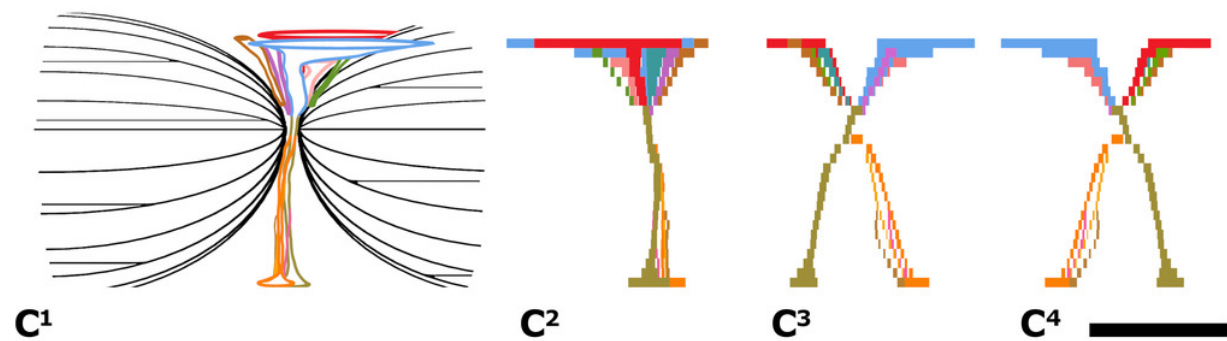
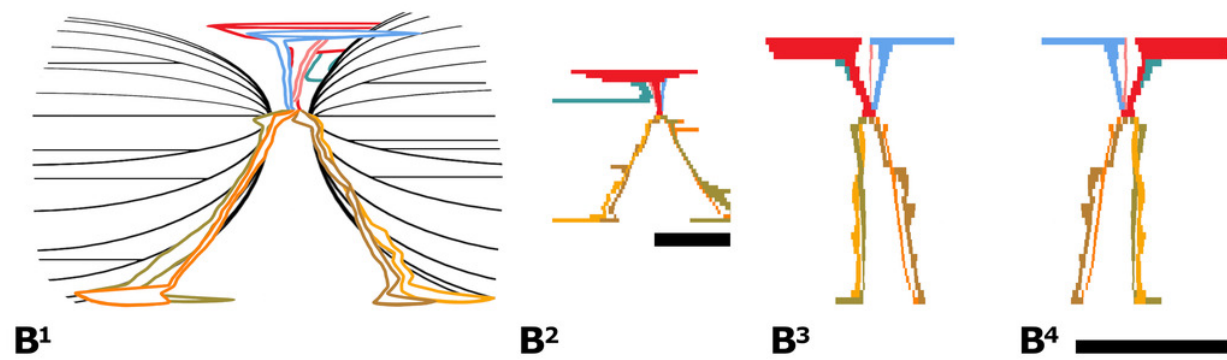
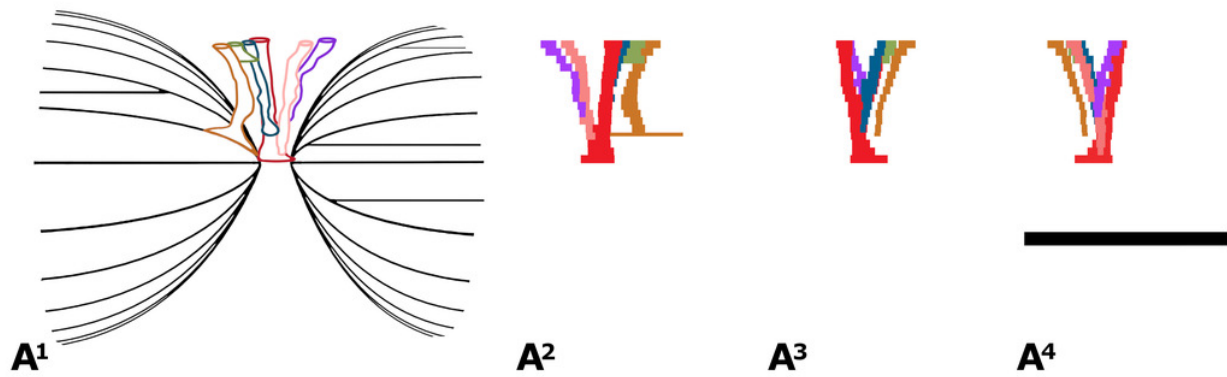


Figure 16

Epiconal vascular canals (epiconal VC), surrounding vertebra's coni.

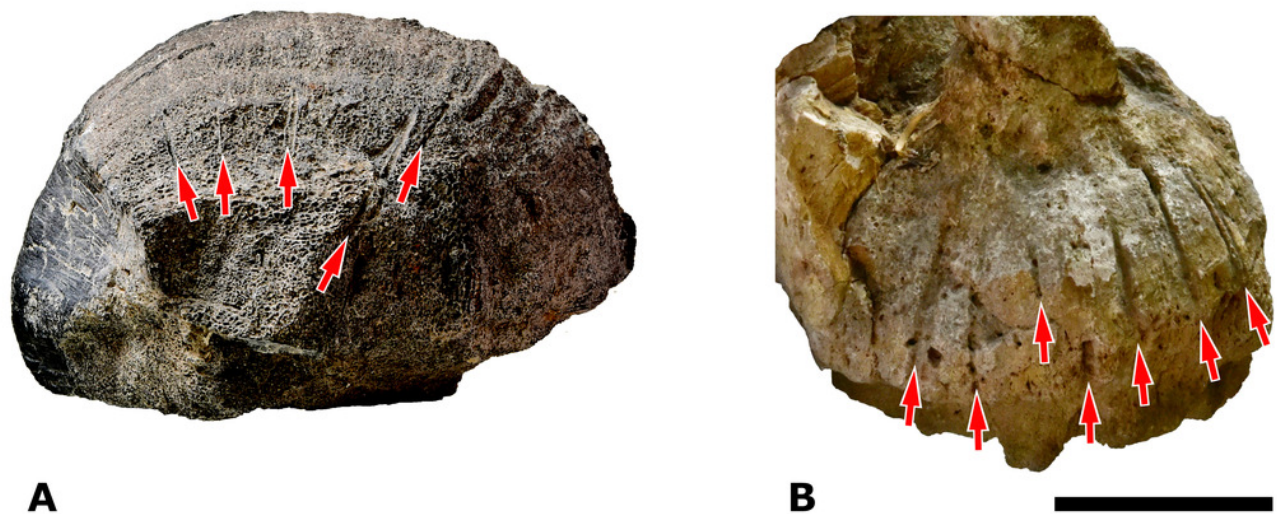


Figure 17

Epiconal vascular canals (epiconal VC).

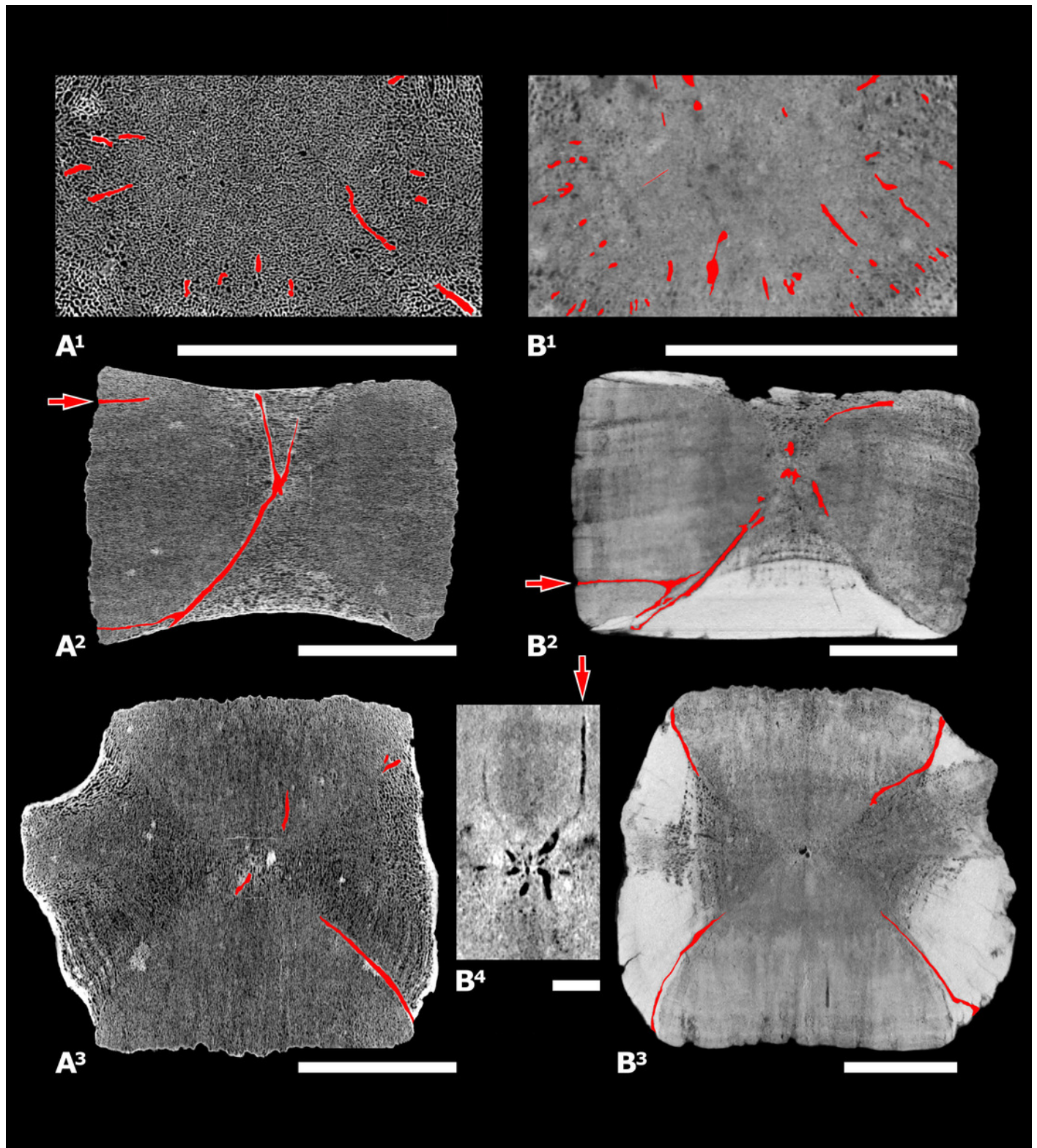


Figure 18

Epiconal vascular canals (epiconal VC).

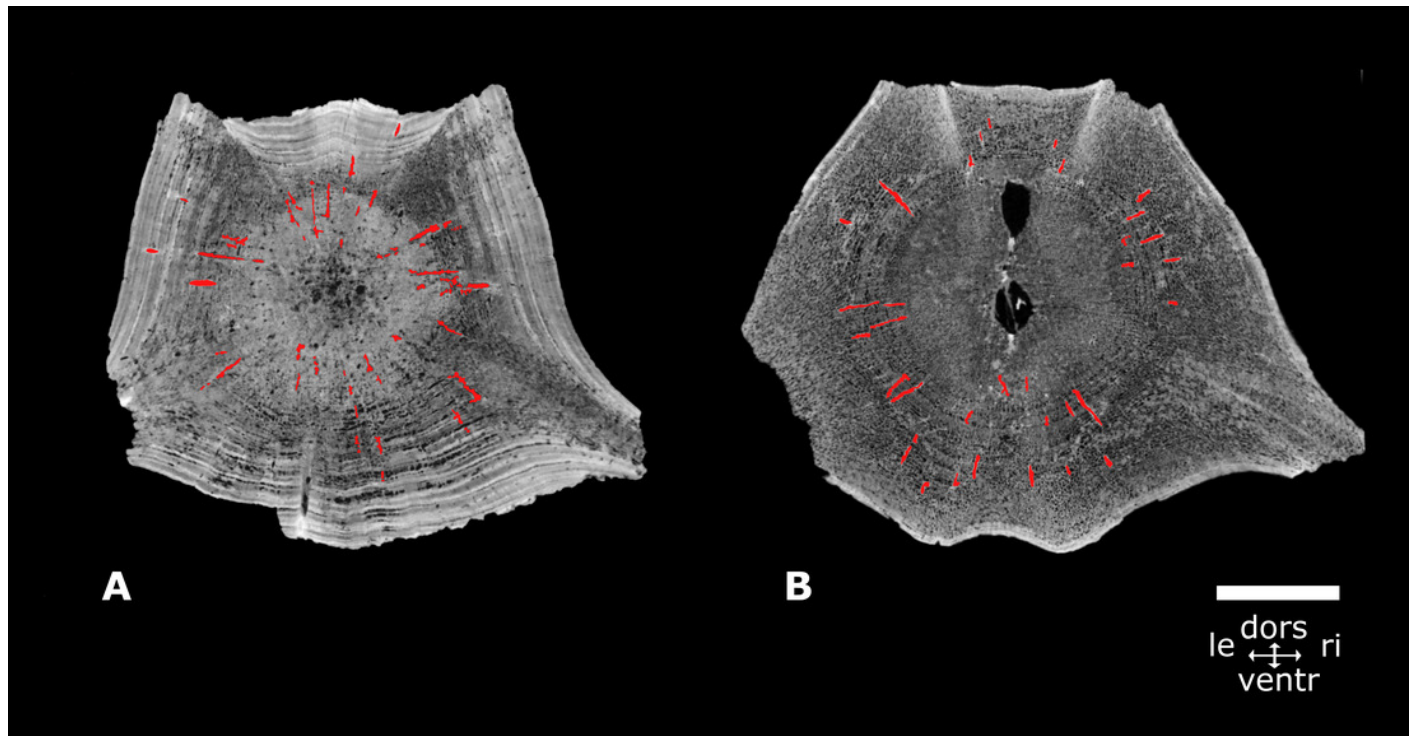


Figure 19

Endoconal vascular canals (endoconal VC).

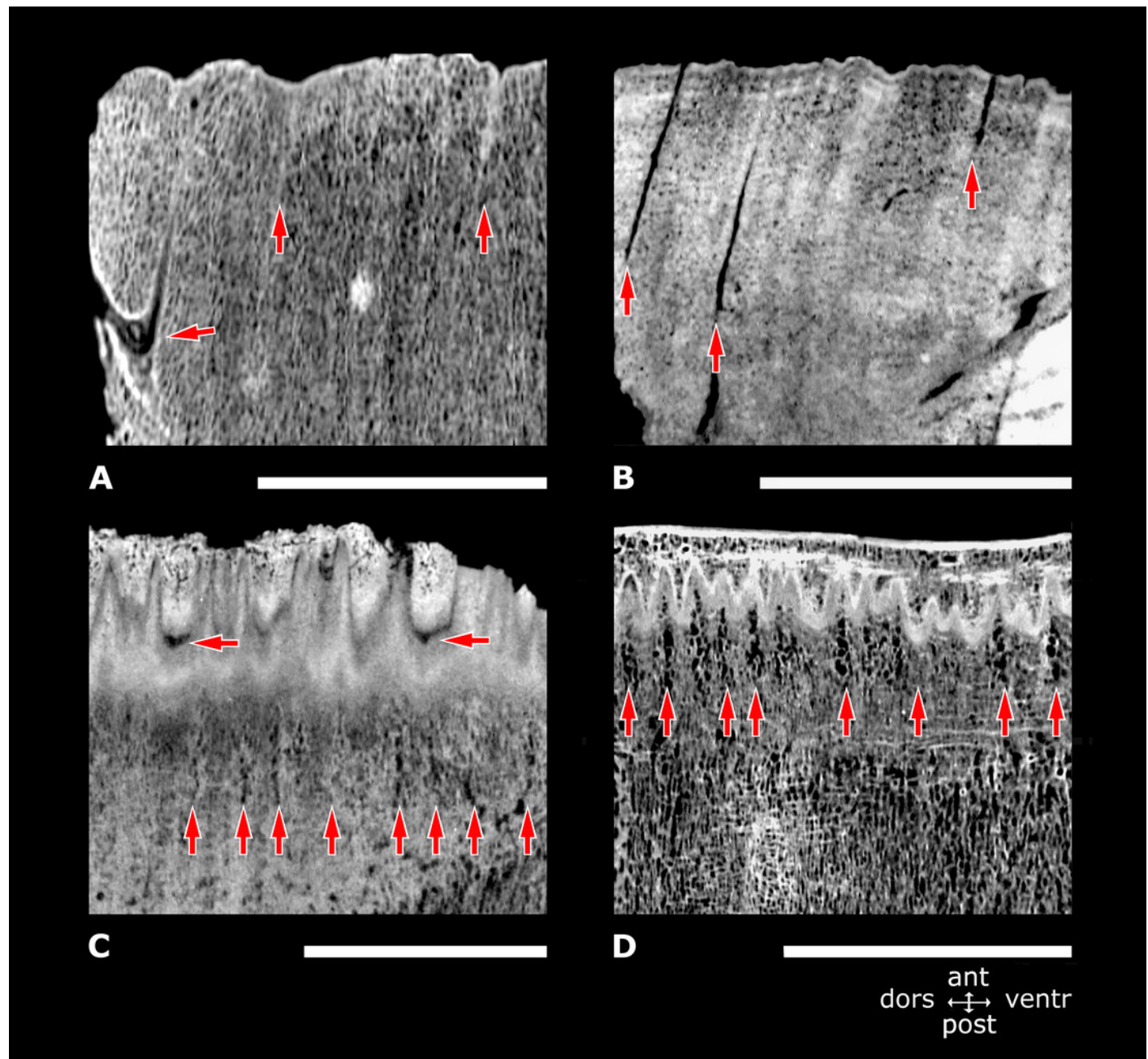
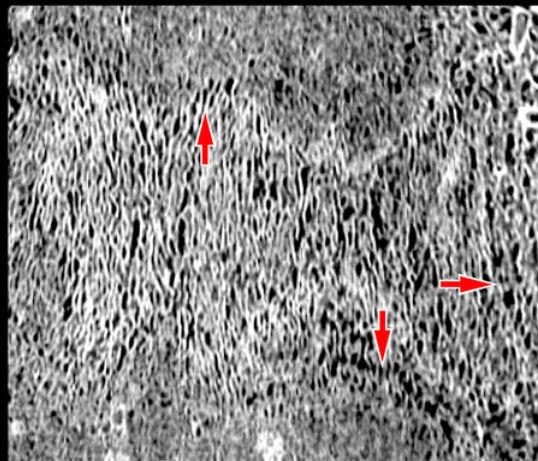
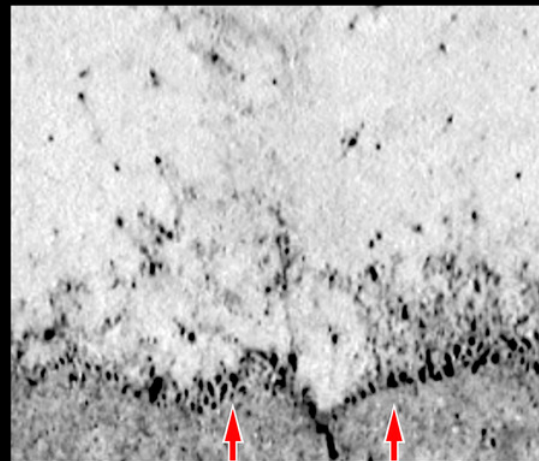


Figure 20

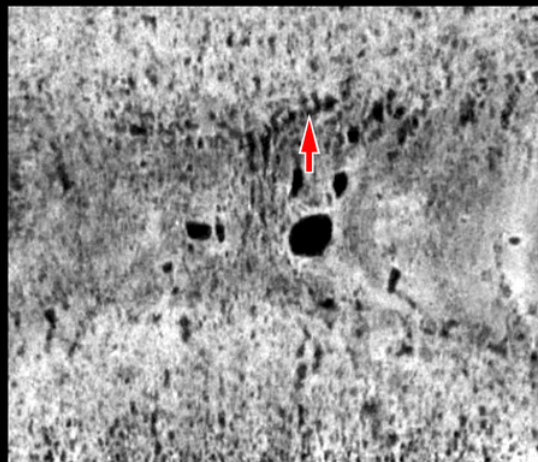
Endocortical vascular canals (endocortical VC).



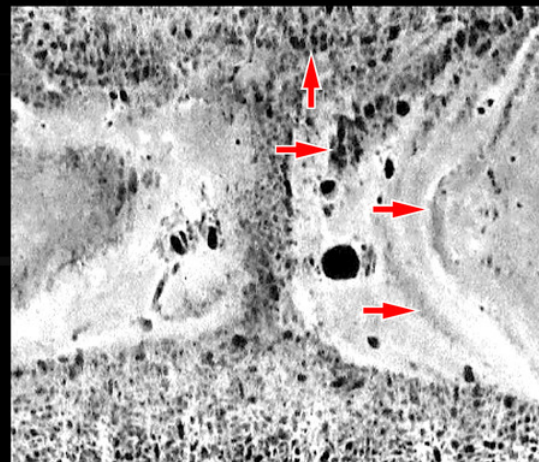
A 



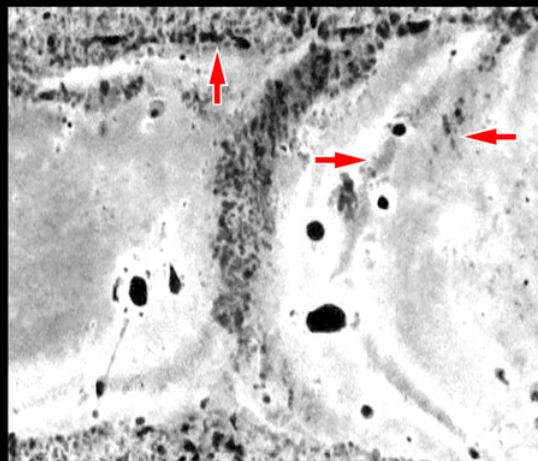
B 



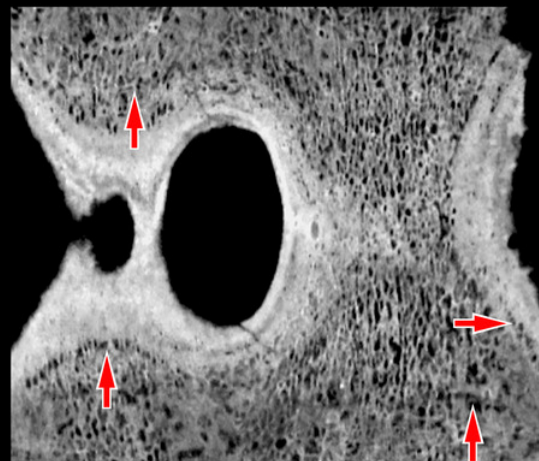
C¹ 



C² 



C³ 



D 

le ant ri
post

Figure 21

Endocortical vascular canals in transverse processes (endocortical VC).

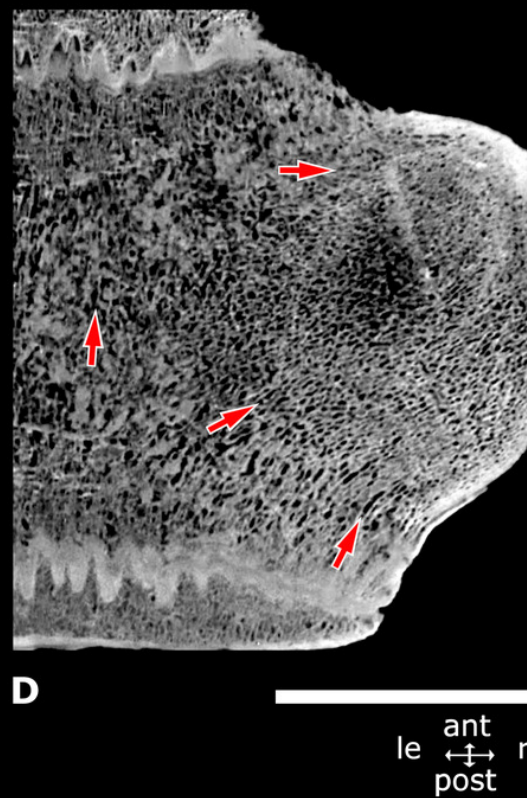
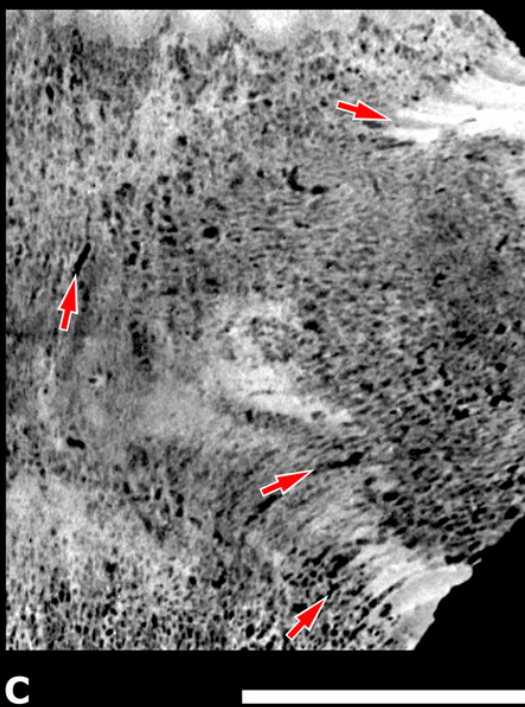
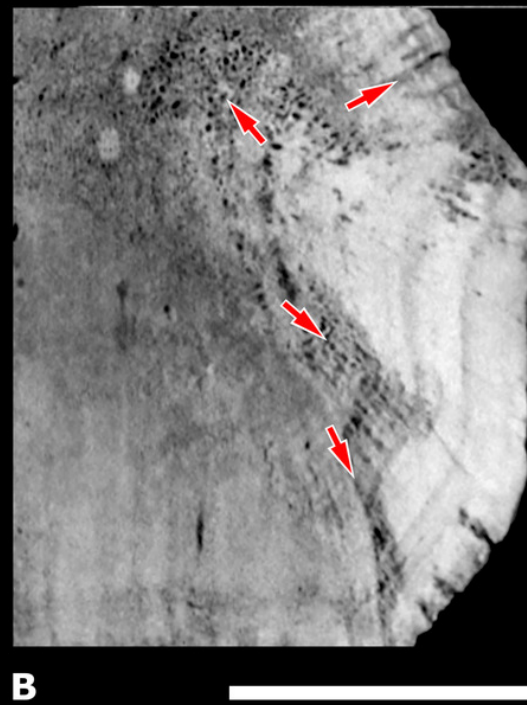


Figure 22

. Accessory vascular canals (accessory VC).

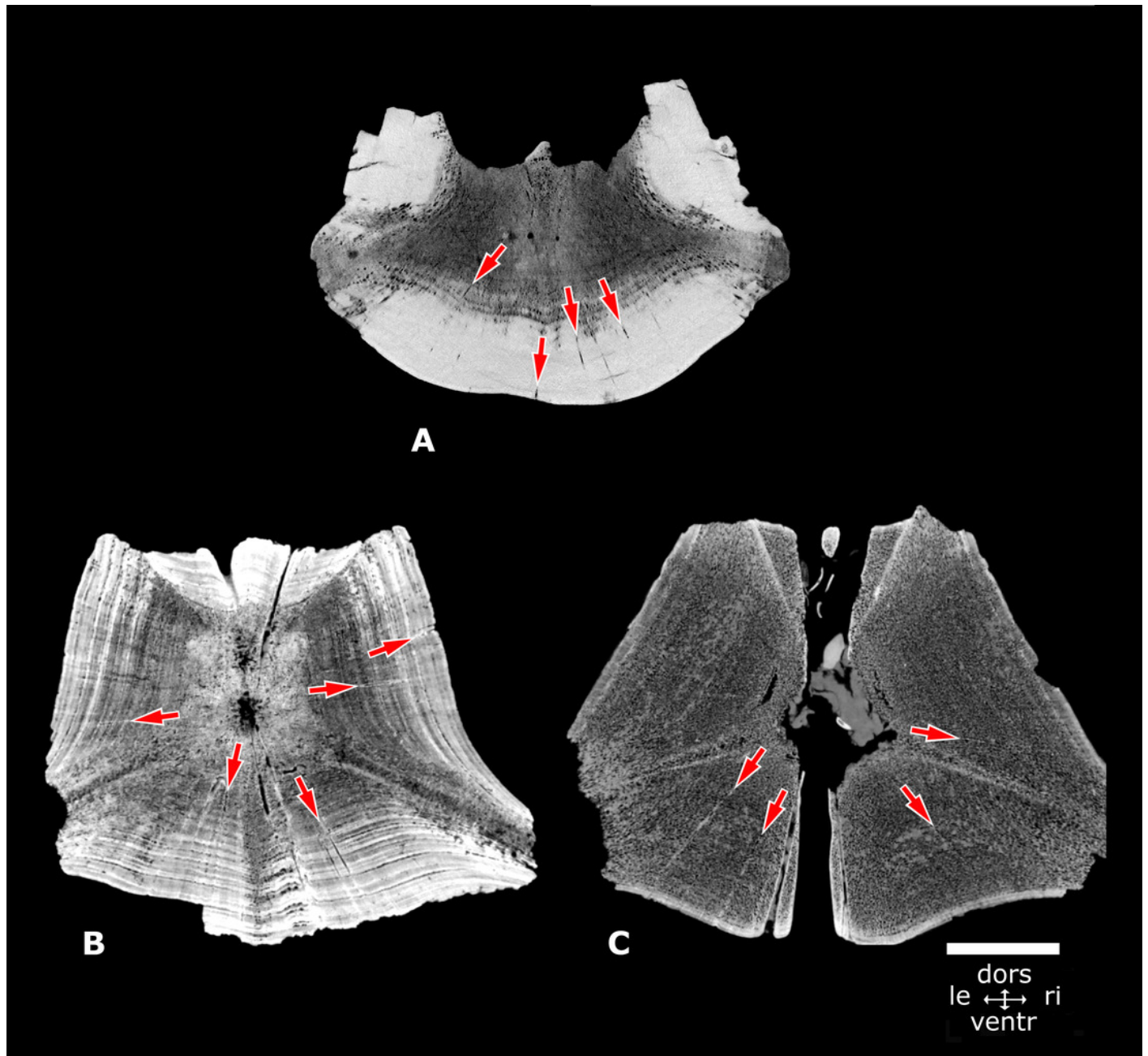


Figure 23

Vascularisation in human vertebrae.

